

VALIDATED COMPUTATION OF HETEROCLINIC SETS

MACIEJ J. CAPIŃSKI * AND J.D. MIRELES JAMES †

Abstract. In this work we develop a method for computing mathematically rigorous enclosures of some one dimensional manifolds of heteroclinic orbits for nonlinear maps. Our method exploits a rigorous curve following argument build on high order Taylor approximation of the local stable/unstable manifolds. The curve following argument is a uniform interval Newton method applied on short line segments. The definition of the heteroclinic sets involve compositions of the map and we use a Lohner-type representation to overcome the accumulation of roundoff errors. Our argument requires precise control over the local unstable and stable manifolds so that we must first obtain validated a-posteriori error bounds on the truncation errors associated with the manifold approximations. We illustrate the utility of our method by proving some computer assisted theorems about heteroclinic invariant sets for a volume preserving map of \mathbb{R}^3 .

Key words. invariant manifolds, heteroclinic orbits, rigorous enclosure of level sets, computer assisted proof, validated numerics, parameterization method, Newton's method

AMS subject classifications. 34C30, 34C45, 37C05, 37D10, 37M99, 65G20, 70K44.

1. Introduction. The study of a nonlinear dynamical system begins by considering the fixed/periodic points, their linear stability, and their local stable and unstable manifolds. In order to patch this local information into a global picture of the dynamics one then wants to understand the connecting orbits. Questions about connecting orbits are naturally reformulated as questions about where and how the stable and unstable manifolds intersect.

A typical situation is that we consider a hyperbolic fixed point, so that the dimension of the stable manifold plus the dimension of the unstable manifold add up to the dimension of the whole space. A transverse intersection of the stable/unstable manifolds of a hyperbolic fixed point is again a single point. Such intersections give rise to homoclinic connecting orbits, and they are of special interest. For example Smale's tangle theorem says that the existence of a transverse homoclinic intersection point implies the existence of hyperbolic chaotic motions [1].

More generally, consider a pair of distinct fixed points and assume that the dimensions s and u of their stable and unstable manifolds have $s + u = d > k$, with k being the dimension of the ambient space. In this case a transverse intersection of the manifolds results in a set which is (locally) a $d - k$ dimensional manifold of connecting orbits. For example we are sometimes interested in transport barriers or separatrices formed by codimension one stable or unstable manifolds [2].

In the present work we develop a computer assisted argument for proving the existence of one dimensional intersections between stable/unstable manifolds of distinct fixed points. Our arguments utilize the underlying dynamics of the map in order to obtain the alpha/omega limit sets of the intersection manifolds. In addition to abstract existence results our argument yields error bounds on the location of the

*AGH University of Science and Technology, Faculty of Applied Mathematics, al. Mickiewicza 30, 30-059 Kraków. Email: mcapinski@agh.edu.pl. The work was partially supported by the Polish National Science Center grant 2012/05/B/ST1/00355.

†Florida Atlantic University, Department of Mathematical Sciences, 777 Glades Rd, Boca Raton, FL 33431, United States. Email: jmirelesjames@fau.edu. The work was partially supported by NSF grant DMS - 1318172.

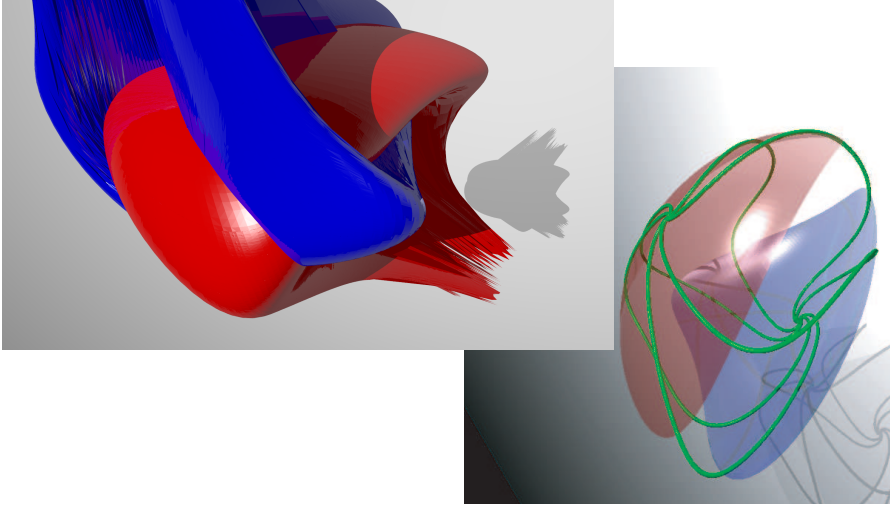


FIG. 1.1. *Heteroclinic intersection arcs for the Lomelí map (see Equation (2.1)). Unstable manifolds in blue, stable manifolds in red, intersection curves in green. The intersection of the manifolds yields six distinct curves. Every point on a curve is a heteroclinic orbit. (All references to color refer to the online version).*

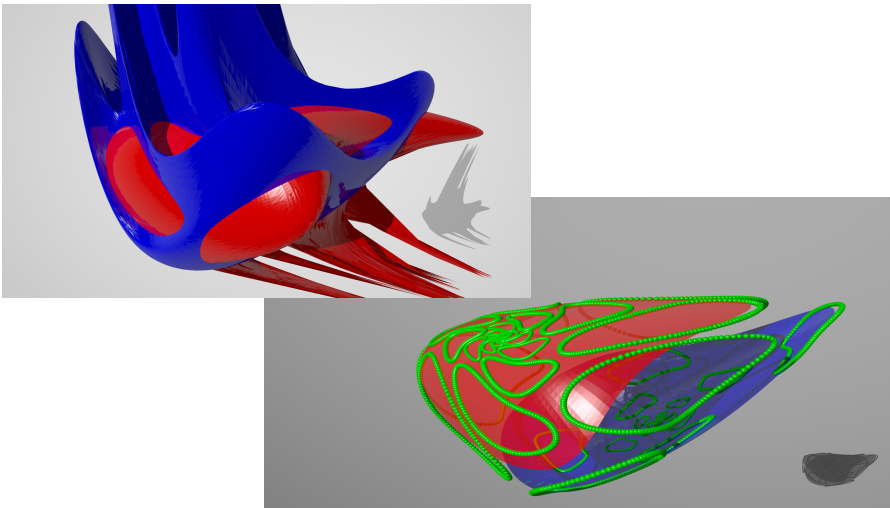


FIG. 1.2. *Heteroclinic intersection loops for the Lomelí map (see Equation (2.1)). Unstable manifolds in blue, stable manifolds in red, intersection curves in green. The intersection of the manifolds yields a countable system of loops. Every point on a loop is a heteroclinic orbit. (All references to color refer to the online version).*

intersection in phase space. Moreover we see that transversality of the intersections follows as a natural corollary, so that the heteroclinic intersections we obtain are in fact normally hyperbolic invariant manifolds.

The two main ingredients in our argument are high order numerical computation of the local stable/unstable manifolds with mathematically rigorous bounds on the truncation error, and a validated branch following algorithm used to rigorously enclose the intersections of these manifolds. Our treatment of the stable/unstable manifolds

is based on the Parameterization method for invariant manifolds [3, 4, 5, 6, 7]. The Parameterization Method is a general functional analytic framework for studying invariant manifolds which reduces questions about the manifold to questions about the solutions of a certain nonlinear operator equation. Reformulating the problem in terms of an operator equation facilitates the design of efficient numerical algorithms for computing the manifold, and introduces a notion of a-posteriori error for the numerical approximations. A-posteriori analysis of the operator leads to computer assisted bounds on the truncation errors.

Next we use these parametric representations of the local stable/unstable manifolds to recast the desired heteroclinic intersection as the one-dimensional zero set of a certain finite dimensional map. An approximate zero set is computed numerically via a Newton/continuation scheme, and a uniform Newton-Krawczyk argument is applied along the $d - k$ dimensional approximate zero set yields a mathematically rigorous enclosure of the true solution. This validated branch following is complicated by the fact that the finite dimensional map contains terms given by multiple compositions of the underlying nonlinear dynamical system. A carefully chosen coordinate system is defined along the branch which allows us to mitigate the so called “wrapping effect”. We mention that a number of other authors have developed methods for validated computation of zero sets, and refer the interested reader to the works of [8, 9, 10, 11, 12, 13], and the references discussed therein for a more complete overview of the literature.

We illustrate our method in a concrete example, and study some global heteroclinic sets in \mathbb{R}^3 , which are defined as the transverse intersection of the unstable and stable manifolds for a pair of distinct fixed points of the *Lomelí map*. This map is defined by Equation (2.1) in Section 2.4, where we discuss the map and its dynamics in more detail. Figures 1.1 and 1.2 illustrate the unstable and stable manifolds, as well as their intersections, for two different choices of parameters for the Lomelí map.

Figure 1.1 illustrates the map with parameter values $a = 0.44$, $b = 0.21$, $c = 0.35$, $\alpha = -0.25$, and $\tau = -0.3$. The map with these parameters was also studied in [14]. The upper left frame suggests that the intersection of $W^u(p_1)$ and $W^s(p_2)$ is a system of arcs beginning and ending at the fixed points. The numerically computed intersection of the manifolds is shown as a collection of green points in the lower right frame. In Section 4 (see Section 4.3.2, in particular) we prove the existence of two distinct intersection arcs whose iterates generate all six curves shown in the lower right frame.

Figure 1.2 illustrates the map with parameter values $a = 0.5$, $b = -0.5$, $c = 1$, $\alpha = -0.08999$, and $\tau = 0.8$. Again, the map with these parameters was also studied in Section 4 of [15], see especially the bottom left frame of figure 4.5 in that reference. For these parameter values the heteroclinic intersections of $W^u(p_1)$ and $W^s(p_2)$ is a system of loops, as we see islands of red surrounded by blue in the upper left frame. The lower right frame illustrates the numerically computed intersection of the manifolds as a collection of green points. In Section 4 (see Section 4.3.1, in particular) we prove the existence of a single intersection loop whose iterates generate the system of loops shown in the lower right frame.

The methods of the present work provide computer assisted proof that the heteroclinic invariant sets suggested by these pictures actually exist. While we implement our methods only for intersection arcs for the Lomelí family in \mathbb{R}^3 , it is clear that the theoretical framework developed here applies much more generally. Indeed, employing the rigorous numerical methods for multiparameter continuation recently developed

in [11] it should be possible to adapt our methods to the study of higher dimensional manifold intersections.

The remainder of the paper is organized as follows. In Section 2 we establish some notation and review some preliminary material including the definitions and basic properties of the stable and unstable manifolds of fixed points, the definitions and basic properties of heteroclinic invariant sets. We also discuss the dynamics of the Lomelí map. In Section 3 we review the basic notions of the Parameterization Methods for stable/unstable manifolds of fixed points, and illustrate the formal computation of the Taylor expansion of the parameterization. We recall an a-posteriori validation theorem which allows us to obtain rigorous computer assisted bounds on the truncation errors. Finally in Section 4 we develop and implment the main tools of the paper, namely the curve following/continuation argument used to enclose the heteroclinic arcs. All of the codes used to obtain the results in this paper can be found at the web page [16].

2. Preliminaries.

2.1. Notations. Throughout this paper we shall use $B_k(x, R)$ to denote a ball of radius R about $x \in \mathbb{R}^k$. To simplify notations we will also write $B_k(R)$ for a ball centered at zero, and B_k for a ball centered at zero with radius 1. Similarly, for $x + iy \in \mathbb{C}$ let $|z| = \sqrt{x^2 + y^2}$ denote the usual absolute value for complex numbers and for $z = (z_1, \dots, z_k) \in \mathbb{C}^k$ define the norm

$$\|z\|_{\mathbb{C}^k} = \max_{1 \leq i \leq k} |z_i|.$$

For $R > 0$ and $z \in \mathbb{C}^k$ let

$$D_k(z, R) = \{w \in \mathbb{C}^k : \|w - z\|_{\mathbb{C}^k} < R\},$$

denote the poly-disk of radius $R > 0$ about $z \in \mathbb{C}^k$. We write $D_k(R)$ for the ball centered at zero and D_k for the unit ball centered at zero.

If we consider $p = (x, y)$, then we will use $\pi_x p$, $\pi_y p$ for the projections onto the x, y coordinates, respectively.

We now write out the interval arithmetic notations conventions that will be used in the paper. Let U be a subset of \mathbb{R}^k . We shall denote by $[U]$ an interval enclosure of the set U , that is, a set

$$[U] = \Pi_{i=1}^k [a_i, b_i] \subset \mathbb{R}^k,$$

such that $U \subset [U]$. Similarly, for a family of matrixes $\mathbf{A} \subset \mathbb{R}^{k \times m}$ we denote its interval enclosure as $[\mathbf{A}]$, that is, a set

$$[\mathbf{A}] = ([a_{ij}, b_{ij}])_{\substack{i=1, \dots, k \\ j=1, \dots, m}} \subset \mathbb{R}^{k \times m},$$

such that $\mathbf{A} \subset [\mathbf{A}]$. For $F : \mathbb{R}^k \rightarrow \mathbb{R}^m$, by $[DF(U)]$ we shall denote an interval enclosure

$$[DF(U)] = \left[\left\{ A \in \mathbb{R}^{k \times m} \mid A_{ij} \in \left[\inf_{x \in U} \frac{\partial F_i}{\partial x_j}(x), \sup_{x \in U} \frac{\partial F_i}{\partial x_j}(x) \right] \right\} \right].$$

For a set U and a family of matrixes \mathbf{A} we shall use the notation $[\mathbf{A}][U]$ to denote an interval enclosure

$$[\mathbf{A}][U] = [\{Au : A \in [\mathbf{A}], u \in [U]\}].$$

We shall say that a family of matrixes $\mathbf{A} \subset \mathbb{R}^{k \times k}$ is invertible, if each matrix $A \in \mathbf{A}$ is invertible. We shall also use the notation

$$[\mathbf{A}]^{-1}[U] = [\{A^{-1}u : A \in [\mathbf{A}], u \in [U]\}].$$

2.2. Stable/unstable manifolds of fixed points. The material in this section is standard and can be found in any textbook on the qualitative theory of dynamical systems. We refer for example to [17, 18]. Let $f: \mathbb{C}^k \rightarrow \mathbb{C}^k$ be a smooth (in our case analytic) map and assume that $p \in \mathbb{C}^k$ is a fixed point of f . Let $U \subset \mathbb{C}^k$ be a neighborhood of p , and define the set

$$W_{\text{loc}}^s(p, U) = \{w \in U : f^n(w) \in U \text{ for all } n \geq 0\}.$$

This set is referred to as the local stable set of p relative to U .

If p is a hyperbolic fixed point, i.e. if none of the eigenvalues of $Df(p)$ are on the unit circle, then the stable manifold theorem gives that there exists a neighbourhood $U \subset \mathbb{C}^k$ of p so that $W_{\text{loc}}^s(p, U)$ is an m -dimensional embedded disk tangent to the stable eigenspace at p . If f is analytic then the embedding is analytic.

The invariant set

$$W^s(p) = \left\{w \in \mathbb{R}^n : \lim_{n \rightarrow \infty} f^n(w) = p\right\},$$

is the stable manifold of p , and consists of all orbits which accumulate under forward iteration of the map to the fixed point p . If f is invertible then we have that

$$W^s(p) = \bigcup_{n=0}^{\infty} f^{-n}[W_{\text{loc}}^s(p, U)],$$

i.e. the stable manifold is obtained as the union of all backwards iterates of a local stable manifold.

We say that the sequence $\{x_j\}_{j=-\infty}^0$ is a backward orbit of x_0 if

$$f(x_j) = x_{j+1},$$

for all $j \leq -1$. If $U \subset \mathbb{R}^k$ and $x_j \in U$ for all $j \leq 0$ we say that x_0 has a backward orbit in U . If

$$\lim_{j \rightarrow -\infty} x_j = p,$$

we say that x_0 has a backward orbit accumulating at p . Let $U \subset \mathbb{C}^k$ be an open neighborhood of p and define the set

$$W_{\text{loc}}^u(p, U) = \{w \in U : w \text{ has a backward orbit in } U\}.$$

We refer to this as a local unstable manifold of p relative to U . If p is hyperbolic, then the unstable manifold theorem gives that there exists an open neighborhood U of p so that $W_{\text{loc}}^u(p, U)$ is a $k - m$ dimensional embedded disk, tangent at p to the unstable eigenspace of $Df(p)$. If f is analytic the embedding is analytic. If f is invertible then the unstable manifold of p under f can be seen as the stable manifold of p under f^{-1} . In the case that f is invertible, the unstable manifold of p is

$$\begin{aligned} W^u(p) &= \left\{w \in \mathbb{R}^n : \lim_{n \rightarrow \infty} f^{-n}(w) = p\right\} \\ &= \bigcup_{n=0}^{\infty} f^n[W_{\text{loc}}^u(p, U)]. \end{aligned}$$

2.3. Heteroclinic Arcs. Suppose that p_1, p_2 are hyperbolic fixed points of an invertible map $f: \mathbb{R}^k \rightarrow \mathbb{R}^k$, and that the invariant manifolds $W^u(p_1)$ and $W^s(p_2)$ are of dimension u_1 and s_2 respectively. Assume that $u_1 + s_2 = k + 1$. If q is a point in the transverse intersection of $W^u(p_1)$ and $W^s(p_2)$ it then follows that there is an arc $\gamma: [-a, a] \rightarrow \mathbb{R}^k$ having that $\gamma(0) = q$ and that

$$\gamma(s) \subset W^u(p_1) \cap W^s(p_2), \quad \text{for all } s \in [-a, a].$$

Moreover this intersection is transverse, hence γ is as smooth as f . We refer to γ as a *heteroclinic arc*.

Since the point $\gamma(s)$, $s \in [-a, a]$ is heteroclinic from p_1 to p_2 , it follows that the set

$$\mathcal{S}(\gamma) = \bigcup_{n \in \mathbb{Z}} f^n(\gamma) \subset W^u(p_1) \cap W^s(p_2),$$

is invariant. Moreover the entire set is heteroclinic from p_1 to p_2 so that

$$\overline{\mathcal{S}(\gamma)} = \mathcal{S}(\gamma) \cup \{p_1\} \cup \{p_2\},$$

i.e. $\mathcal{S}(\gamma)$ accumulates only at the fixed points. Then $\overline{\mathcal{S}(\gamma)}$ is a compact invariant set. We refer to $\overline{\mathcal{S}(\gamma)}$ as the heteroclinic invariant set generated by γ .

Suppose that γ can be continued to a longer curve $\tilde{\gamma}$, i.e. suppose that there is $\tilde{\gamma}: [-b, b] \rightarrow \mathbb{R}^k$ with $a < b$ and $\gamma = \tilde{\gamma}|_{[-a, a]}$. Then

$$\overline{\mathcal{S}(\gamma)} \subset \overline{\mathcal{S}(\tilde{\gamma})}.$$

We are interested in the largest compact invariant set so obtained, and single out two cases of particular interest.

DEFINITION 2.1 (fundamental heteroclinic loop). Suppose that $\gamma(-a) = \gamma(a)$, i.e. γ is a closed loop. Then the heteroclinic invariant set $\mathcal{S}(\gamma)$ is the union of countably many closed loops accumulating at p_1 and p_2 . If each point $q \in \gamma$ is a point of transverse intersection of $W^u(p_1)$ and $W^s(p_2)$ then the closed loop γ has no self intersections. Moreover the lack of self intersections propagates under forward and backward iteration as f is a diffeomorphism. In this case we refer to γ as a *fundamental heteroclinic loop*.

An example of a heteroclinic loop connection for the Lomelí map is given in Figure 1.2. This connection is generated by a single loop, propagated under forward and backward iterations of f .

DEFINITION 2.2 (m -fold fundamental heteroclinic arc). If $\gamma(a) = f^m(\gamma(-a))$ for some $m \geq 1$ and $f^i(\gamma(-a)) \notin \gamma$ for $i < m$, then the m -th iterate of the arc γ is a continuation of γ . (If $f^m(\gamma(a)) = \gamma(-a)$ then reparameterize.) We refer to γ as an *m -fold fundamental heteroclinic arc*. Now

$$\mathcal{S}_m(\gamma) := \bigcup_{i \in \mathbb{Z}} f^{im}(\gamma)$$

is itself an arc connecting p_1 and p_2 , which we refer to as the *heteroclinic path generated by γ* .

For any $j \in \{1, \dots, m-1\}$ the set $f^j(\mathcal{S}_m(\gamma))$ is another heteroclinic path from p_1 to p_2 . If each point $q \in \gamma$ is a point of transverse intersection of $W^u(p_1)$ and $W^s(p_2)$

then for each $j \in \{1, \dots, m-1\}$, the sets $f^i(\mathcal{S}_m(\gamma))$, $f^{i+j}(\mathcal{S}_m(\gamma))$ are disjoint. We refer to

$$\overline{\mathcal{S}(\gamma)} = \bigcup_{j=0}^{m-1} f^j(\overline{\mathcal{S}_m(\gamma)}) = \bigcup_{i \in \mathbb{Z}} f^i(\gamma) \cup \{p_1\} \cup \{p_2\},$$

as an *m-fold heteroclinic branched manifold*, as $\overline{\mathcal{S}(\gamma)}$ is composed of m paths (or branches).

An example of a heteroclinic branched manifold for the Lomelí map is given in Figure 1.1. It consists of six paths, which are generated by two distinct 3-fold fundamental heteroclinic arcs.

In both the case of the heteroclinic arcs, and the case of heteroclinic loops, the compact invariant sets $\overline{\mathcal{S}(\gamma)}$ are maximal with respect to γ , in the sense that no larger invariant set can be obtained by continuation of the arc γ . In either case we refer to γ as a *fundamental heteroclinic arc*. Note that under the assumption that γ arises as the one dimensional transverse intersection of smooth manifolds, the classification theorem for one dimensional manifolds gives that only these two cases occur.

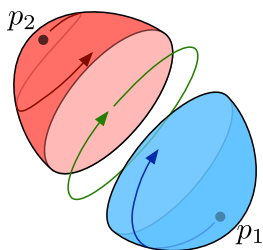


FIG. 2.1. *Vortex bubble: in this sketch p_1 and p_2 are hyperbolic fixed points with two dimensional unstable and two dimensional stable manifolds respectively. The indicated unstable and stable eigenvalues occur in complex conjugate pairs, giving the system a “twist” or circulation at the fixed points. The circulation is sympathetic (clockwise or counterclockwise at p_1 and p_2) and in the region between the fixed points there is a “vortex”.*

2.4. Vortex bubbles and the Lomelí map. In the sequel we restrict our attention to a particular dynamical configuration known as a *vortex bubble*. Heteroclinic arcs play an important role in the study of vortex bubbles, and vortex bubbles in \mathbb{R}^3 provide a non-trivial application, which can still be completely visualized. Vortex bubbles appear in the fluid dynamics and plasma physics literature as a model of turbulent circulation. See for example [19, 20, 21] and the references discussed therein. At present we provide a brief qualitative sketch sufficient to our needs.

The main features of a vortex bubble are as follows. Consider $f: \mathbb{R}^3 \rightarrow \mathbb{R}^3$ a volume preserving diffeomorphism (which could arise as a time one map of a volume preserving flow) having a pair of distinct hyperbolic fixed points $p_1, p_2 \in \mathbb{R}^3$. We suppose that p_1 has two dimensional unstable manifold, and that p_2 has two dimensional stable manifold. Moreover we suppose that the unstable eigenvalues at p_1 and the stable eigenvalues at p_2 occur in complex conjugate pair, hence the linear dynamics at each fixed point is rotational.

We assume that the rotation is in the same direction at the fixed points, and also that the curvature at p_1 and p_2 of the local unstable/stable manifolds is such that the manifolds bend or “cup” toward one another. Should the two dimensional global stable/unstable manifolds enclose a region we say that a bubble (or resonance bubble) is formed. Under these conditions it is not unusual that the circulation at the fixed points drives a circulation throughout the bubble, in which case we say that there is a vortex bubble. Inside the vortex bubble one may find invariant circles and tori, as well as complicated chaotic motions.

The situation just described is sketched in Figure 2.4. An important global consideration is the intersection of the two dimensional unstable and stable manifolds which, if transverse, gives rise to heteroclinic arcs as discussed in Section 2.3.

One elementary mathematical model exhibiting vortex bubble dynamics is the five parameter family of quadratic volume preserving maps

$$f(x, y, z) = \begin{pmatrix} z + \alpha + \tau x + ax^2 + bxy + cy^2 \\ x \\ y \end{pmatrix}, \quad (2.1)$$

with $a + b + c = 1$. We refer to this as the Lomelí family, or simply as the Lomelí map. The map is a natural generalization of the Hénon map from two to three dimensions, and is the subject of a number of studies [22, 23, 24, 15]. In particular the Lomelí map provides a normal form for volume preserving quadratic diffeomorphisms with quadratic inverse, and is a toy model for turbulent fluid/plasma flow near a vortex [23, 15, 14, 25].

For typical parameters the map has two hyperbolic fixed points p_1 and p_2 with stability as discussed above. The global embedding of the stable and unstable manifolds for the system is illustrated in two specific instances in Figures 1.1 and 1.2 of the Introduction. These computations suggest that both case 1 of heteroclinic arcs (in this case) 3-fold, and case 2 of heteroclinic loops occur for the system as defined in Section 2.3 occur for the Lomelí map. In the sequel we prove, by a computer assisted argument, that this is indeed the case.

3. Review of the parameterization method for stable/unstable manifolds of fixed points. Let $f: \mathbb{C}^k \rightarrow \mathbb{C}^k$ be a smooth map and suppose that $p \in \mathbb{C}^k$ is a hyperbolic fixed point as in Section 2.2. Then the eigenvalues $\lambda_1, \dots, \lambda_k \in \mathbb{C}$ for $Df(p)$ have

$$|\lambda_j| \neq 1, \quad \text{for all } 1 \leq j \leq k,$$

i.e. none of the eigenvalues are on the unit circle. Let $\lambda_1, \dots, \lambda_s \in \mathbb{C}$ denote the stable eigenvalues of $Df(p)$, where $s \leq k$. We order the stable eigenvalues so that

$$|\lambda_s| \leq \dots \leq |\lambda_1| < 1,$$

and so that λ_j is unstable when $s < j \leq k$.

For the sake of simplicity, suppose that $Df(p)$ is diagonalizable and let $\xi_1, \dots, \xi_k \in \mathbb{C}^k$ denote a choice of associated eigenvectors. Then

$$Df(p) = Q\Lambda Q^{-1},$$

where

$$\Lambda = \begin{pmatrix} \lambda_1 & \dots & 0 \\ \vdots & \ddots & \vdots \\ 0 & \dots & \lambda_k \end{pmatrix},$$

is the $k \times k$ diagonal matrix of eigenvalues and

$$Q = [\xi_1, \dots, \xi_k],$$

is the $k \times k$ matrix whose j -th column is the eigenvector associated with λ_j . We write

$$\Lambda_s = \begin{pmatrix} \lambda_1 & \dots & 0 \\ \vdots & \ddots & \vdots \\ 0 & \dots & \lambda_s \end{pmatrix},$$

to denote the $s \times s$ diagonal matrix of stable eigenvalues.

In the present work we assume that f is analytic in a neighborhood of p . Let

$$D_s = \{\mathbf{z} = (z_1, \dots, z_s) \in \mathbb{C}^s : |z_j| < 1 \text{ for each } 1 \leq j \leq s\},$$

denote the s -dimensional unit poly-disk in \mathbb{C}^s . The goal of the Parameterization Method is to find an analytic map $P: D_s \rightarrow \mathbb{C}^k$ having that

$$P(0) = p, \quad DP(0) = [\xi_1, \dots, \xi_s], \quad (3.1)$$

and

$$f[P(z_1, \dots, z_s)] = P(\lambda_1 z_1, \dots, \lambda_s z_s), \quad (3.2)$$

for all $(z_1, \dots, z_s) \in D_s$. Such a map P parameterizes a local stable manifold for f at p , as the following lemma makes precise.

LEMMA 3.1. *Suppose that P is an analytic map satisfying the first order constraints in (3.1) and solving Equation (3.2) in $D_s \subset \mathbb{C}^s$. Then P is a chart map for a local stable manifold at p , i.e.*

1. *for all $z \in P[D_s]$ the orbit of z accumulates at p ,*
2. *$P[D_s]$ is tangent to the stable eigenspace at p ,*
3. *P is one-to-one on D_s , i.e. P is a chart map.*

The proof of Lemma 3.1 follows along the same lines as Section 3.1 of [15]. Here we sketch the argument: Point 1. is seen by iterating the invariance equation (3.2), considering the continuity of P and the requirement that $P(0) = p$. Point 2. follows directly from the first order constraint on $DP(0)$ given in Equation (3.1), and point 3. is seen by applying the implicit function theorem to show that P is one-to-one in a small neighborhood of the origin in D_s , and then using that f and Λ_s are invertible maps to show that P is one-to-one anywhere that Equation (3.2) holds.

Since we seek P analytic on a disk and satisfying first order constraints its natural to look for a power series representation

$$P(z_1, \dots, z_s) = \sum_{\alpha_1=0}^{\infty} \dots \sum_{\alpha_s=0}^{\infty} p_{\alpha_1, \dots, \alpha_s} z_1^{\alpha_1} \dots z_s^{\alpha_s} = \sum_{|\alpha|=0}^{\infty} p_{\alpha} z_{\alpha}, \quad (3.3)$$

where $\alpha = (\alpha_1, \dots, \alpha_s) \in \mathbb{N}^s$ is an s -dimensional multi-index,

$$|\alpha| = \alpha_1 + \dots + \alpha_s,$$

$p_{\alpha_1, \dots, \alpha_s} = p_{\alpha} \in \mathbb{C}^k$ for each $\alpha \in \mathbb{N}^s$, and $z^{\alpha} = z_1^{\alpha_1} \dots z_s^{\alpha_s} \in \mathbb{C}$ for each $z \in D_s$, $\alpha \in \mathbb{N}^s$. Imposing the first order constraints (3.1) gives

$$p_{0, \dots, 0} = 0, \quad \text{and} \quad p_{e_j} = \xi_j,$$

where for each $1 \leq j \leq s$ the multi-index e_j is given by $e_j = (0, \dots, 1, \dots, 0)$, i.e. e_j has a one in the j -th entry and zeros elsewhere. The Taylor coefficients p_α for $|\alpha| \geq 2$ can be determined by a power matching scheme. This procedure is illustrated by example in the next section.

REMARK 3.2 (Unstable manifold parameterization). The considerations above apply to the unstable manifold of f at p by considering the stable manifold of the inverse map f^{-1} at p . In fact the equation becomes

$$f^{-1}[P(z_1, \dots, z_u)] = P(\sigma_1 z_1, \dots, \sigma_u z_u),$$

where u is the number of stable eigenvalues of $Df^{-1}(p)$ and $\sigma_1, \dots, \sigma_u$ denote these stable eigenvalues. Of course the stable eigenvalues for $Df^{-1}(p)$ are the reciprocals of the unstable eigenvalues for $Df(p)$ so that $u = k - s$. Applying f to both sides of the equation and pre-composing P with $\sigma_1^{-1}, \dots, \sigma_u^{-1}$ we obtain

$$P(\sigma_1^{-1} z_1, \dots, \sigma_u^{-1} z_u) = f[P(z_1, \dots, z_u)],$$

with $\sigma_i^{-1} = \lambda_i$ the unstable eigenvalues of $Df(p)$. This shows that chart maps for the stable and unstable manifolds satisfy the same Equation (3.2). The difference is that in one case we conjugate to the linear map given by the stable eigenvalues of $Df(p)$ and in the other case the linear map given by the unstable eigenvalues.

3.1. Example: 2D manifolds associated with complex conjugate eigenvalues for the Lomelí family. In this section we write out in full detail how the parameterization method works on the concrete example of the Lomelí map. We include these formal computations for the sake of completeness.

Suppose that $p \in \mathbb{R}^3$ is a fixed point of the Lomelí map and that $Df(p)$ has a pair of stable complex conjugate eigenvalues $\lambda, \bar{\lambda} \in \mathbb{C}$, i.e. $|\lambda| = |\bar{\lambda}| < 1$. Let $\xi, \bar{\xi} \in \mathbb{C}^3$ denote the complex conjugate eigenvectors. Note that since the Lomelí map is volume preserving, it is the case that the remaining eigenvalue is real and unstable.

Take v, w in the unit disk in \mathbb{C} and write

$$P(v, w) = \begin{pmatrix} P_1(v, w) \\ P_2(v, w) \\ P_3(v, w) \end{pmatrix} = \sum_{k=0}^{\infty} \sum_{l=0}^{\infty} \begin{pmatrix} p_{kl}^1 \\ p_{kl}^2 \\ p_{kl}^3 \end{pmatrix} v^k w^l.$$

We see that

$$P(0, 0) = \begin{pmatrix} p_{00}^1 \\ p_{00}^2 \\ p_{00}^3 \end{pmatrix} = p, \quad \frac{\partial}{\partial v} P(0, 0) = \begin{pmatrix} p_{10}^1 \\ p_{10}^2 \\ p_{10}^3 \end{pmatrix} = \xi, \quad \frac{\partial}{\partial w} P(0, 0) = \begin{pmatrix} p_{01}^1 \\ p_{01}^2 \\ p_{01}^3 \end{pmatrix} = \bar{\xi},$$

by imposing the first order constraints of Equation (3.1). Plugging the unknown power series expansion of P into the invariance Equation (3.2) gives

$$\begin{aligned} f[P(v, w)] &= \\ &= \begin{pmatrix} P_3(v, w) + \alpha + \tau P_1(v, w) + a P_1(v, w)^2 + b P_1(v, w) P_2(v, w) + c P_2(v, w)^2 \\ P_1(v, w) \\ P_2(v, w) \end{pmatrix} \\ &= \sum_{k=0}^{\infty} \sum_{l=0}^{\infty} \begin{pmatrix} p_{kl}^3 + \delta_{kl} \alpha + \tau p_{kl}^1 + \sum_{i=0}^k \sum_{j=0}^l \left(a p_{k-il-j}^1 p_{ij}^1 + b p_{k-il-j}^1 p_{ij}^2 + c p_{k-il-j}^2 p_{ij}^2 \right) \\ p_{kl}^1 \\ p_{kl}^2 \end{pmatrix} v^k w^l, \end{aligned}$$

on the left (where $\delta_{kl} = 0$ if $k = 0$ and $l = 0$ and $\delta_{kl} = 1$ otherwise), and

$$P(\lambda v, \bar{\lambda} w) = \sum_{k=0}^{\infty} \sum_{l=0}^{\infty} \lambda^k \bar{\lambda}^l \begin{pmatrix} p_{kl}^1 \\ p_{kl}^2 \\ p_{kl}^3 \end{pmatrix} v^k w^l,$$

on the right. Matching like powers leads to

$$\begin{pmatrix} p_{kl}^3 + \delta_{kl}\alpha + \tau p_{kl}^1 + \sum_{i=0}^k \sum_{j=0}^l a p_{k-il-j}^1 p_{ij}^1 + b p_{k-il-j}^1 p_{ij}^2 + c p_{k-il-j}^2 p_{ij}^2 \\ p_{kl}^1 \\ p_{kl}^2 \end{pmatrix} = \lambda^k \bar{\lambda}^l \begin{pmatrix} p_{kl}^1 \\ p_{kl}^2 \\ p_{kl}^3 \end{pmatrix}$$

for all $k + l \geq 2$. Extracting terms of order kl and isolating them on the left hand side leads to the linear *homological* equations

$$\begin{bmatrix} \tau + 2a + b - \lambda^k \bar{\lambda}^l & b + 2c & 1 \\ 1 & -\lambda^k \bar{\lambda}^l & 0 \\ 0 & 1 & -\lambda^k \bar{\lambda}^l \end{bmatrix} \begin{pmatrix} p_{kl}^1 \\ p_{kl}^2 \\ p_{kl}^3 \end{pmatrix} = s_{kl}, \quad (3.4)$$

where

$$s_{kl} = \begin{pmatrix} -\sum_{i=0}^k \sum_{j=0}^l \hat{\delta}_{ij} (a p_{k-il-j}^1 p_{ij}^1 + b p_{k-il-j}^1 p_{ij}^2 + c p_{k-il-j}^2 p_{ij}^2) \\ 0 \\ 0 \end{pmatrix}$$

and the coefficient

$$\hat{\delta}_{ij} = \begin{cases} 0 & i = 0 \text{ and } j = 0, \\ 0 & i = k \text{ and } j = l, \\ 1 & \text{otherwise,} \end{cases}$$

accounts for the fact that terms of order kl have been extracted from the sums. In other words: the s_{kl} depend only on terms p_{ij} where $i + j < k + l$.

The question arises: for what k, l with $k + l \geq 2$ does the linear Equation (3.4) have a unique solution? Direct inspection of the formula for $Df(p)$ when f is the Lomelí map allows us to rewrite the homological equation as

$$(Df(p) - \lambda^k \bar{\lambda}^l \text{Id}) p_{kl} = s_{kl}. \quad (3.5)$$

Note that the matrix on the left hand side is characteristic for $Df(p)$. In other words, this matrix is invertible as long as $\lambda^k \bar{\lambda}^l$ is not an eigenvalue of $Df(p)$. Since both $\lambda^k \bar{\lambda}^l = \lambda$ and $\lambda^k \bar{\lambda}^l = \bar{\lambda}$ are impossible for $k + l \geq 2$, and since the remaining eigenvalue is unstable, we see that this matrix is invertible for all cases of concern. Then the Taylor coefficients of P are formally well defined to all orders. Moreover we obtain a numerical algorithm by recursively solving the homological equations to any desired order. We write

$$P^N(v, w) = \sum_{n=0}^N \sum_{k+l=n} p_{kl} v^k w^l,$$

to denote the N -th order polynomial obtained by solving the homological equations to order N . We remark that by solving these homological equations using interval arithmetic we obtain validated interval enclosures of the true coefficients. This discussion goes through unchanged if $\lambda, \bar{\lambda} \in \mathbb{C}$ are unstable rather than stable eigenvalues.

REMARK 3.3. Note that the Lomelí map is real analytic, and for real fixed points $p \in \mathbb{R}^3$ we are interested in the real image of P . Using the fact that $Df(p)$ is a real matrix when p is a real fixed point, we see that

$$\overline{Df(p) - \lambda^k \bar{\lambda}^l \text{Id}} = Df(p) - \bar{\lambda}^k \lambda^l \text{Id},$$

and similarly it is easy to check that $\overline{s_{kl}} = s_{lk}$ for all k, l . Since we choose the first order coefficients so that

$$\overline{p_{10}} = \bar{\xi} = p_{01},$$

it follows that the solutions of all homological equations inherit this property, i.e. that

$$\overline{p_{kl}} = p_{lk}$$

for all $k + l \geq 2$.

Choosing complex conjugate variables

$$v = s + it \quad \text{and} \quad w = s - it,$$

with s, t real we see that the map $\hat{P}: B \rightarrow \mathbb{R}^3$ given by

$$\hat{P}(s, t) = P(s + it, s - it),$$

is real valued. Moreover the constraint that v, w lie in the unit Poly-disk in \mathbb{C}^2 imposes that

$$B_2 = \left\{ (s, t) \in \mathbb{R}^2 : \sqrt{s^2 + t^2} < 1 \right\},$$

is the natural domain for \hat{P} . These remarks show also that the truncated polynomial approximation P^N has complex conjugate coefficients, and hence a real image when we make use the complex conjugate variables, as long as we include each coefficients p_α with $2 \leq |\alpha| \leq N$ in our approximation.

REMARK 3.4 (Uniqueness and decay rate of the coefficients). The discussion of the homological equation above shows that the Taylor coefficients p_{kl} are unique up to the choice of the length of ξ . In fact it can be shown that if \hat{p}_{kl} are the coefficients associated with the scaling $|\xi| = |\bar{\xi}| = 1$, and p_{kl} are the coefficients associated with the scaling $|\xi| = |\bar{\xi}| = \tau$, then we have the relationship

$$p_{kl} = \tau^{k+l} \hat{p}_{kl}.$$

A simple proof of this fact is found for example in [26]. Then the length of ξ adjusts the decay rate of the power series coefficients. This freedom is exploited in order to stabilize numerical computations.

REMARK 3.5 (A-posteriori error). The computations above are purely formal, and in practice we would like to measure the accuracy of the approximation on a fixed domain. In order to make such a measurement we exploit that the lengths of the eigenvectors tune the decay rates of the power series coefficient, so that we can

always fix the domain of P^N to be the unit disk. Equation (3.2) then suggests we define the a-posteriori error functional

$$\epsilon_N = \sup_{|v|, |w| < 1} \|f[P^N(v, w)] - P^N(\lambda v, \bar{\lambda} w)\|_{\mathbb{C}^3}.$$

This quantity provides a heuristic indicator of the quality of the approximation P^N on the unit disk. Of course small defects do not necessarily imply small truncation errors. In Section 3.2 we discuss a method which makes this heuristic indicator precise.

Note that if N is fixed then ϵ_N is a function of the length of ξ only. Then by varying the length we can make ϵ_N as small as we wish (up to machine errors). To see this we simply note that $f \circ P^N$ is exactly equal to $P^N \circ \Lambda_s$ to zero and first order, so that the function $f \circ P^N - P^N \circ \Lambda_s$ is zero to second order and has higher order coefficients decaying as fast as we wish. Once a desired error is achieved fixed we increase N and repeat the procedure. In this way one can optimize the size of the image of P^N relative to a fixed desired error tolerance. Again we refer the interested reader to [26], where such algorithms are discussed in more detail.

REMARK 3.6 (Generalizations). The computations sketched above succeed in much greater generality. For example when we study an m dimensional manifold of an analytic mapping $f: \mathbb{C}^k \rightarrow \mathbb{C}^k$, then looking for a parameterization of the form

$$P(z) = \sum_{|\alpha|=0}^{\infty} p_{\alpha} z^{\alpha},$$

leads to a homological equation of the form

$$[Df(p) - \lambda_1^{\alpha_1} \dots \lambda_s^{\alpha_s} \text{Id}] p_{\alpha} = s_{\alpha},$$

for the coefficients with $|\alpha| \geq 2$. Here again s_{α} depends only on terms of order lower than $|\alpha|$, and the form of s_{α} is determined by the nonlinearity of f . Note that the general case leads to the non-resonance conditions

$$\lambda_1^{\alpha_1} \dots \lambda_s^{\alpha_s} \neq \lambda_j \quad \text{for } 1 \leq j \leq s.$$

Inspection of these conditions shows that the non-resonance conditions hold generically, i.e. they reduce to a finite collection of constraint equations. Moreover, should a resonance occur it is still possible for the Parameterization Method to succeed. However when there is a resonance, rather than conjugating to the linear map generated by the stable eigenvalues, it is necessary to conjugate the dynamics on the manifold to a certain polynomial which “kills” the resonant terms. The general development of the Parameterization Method for stable/unstable manifolds of non-resonant fixed points is in [3, 4, 5]. Validated numerical methods for the resonant case as well as the non-diagonalizable case are developed in [27].

3.2. A-posteriori validation and computer assisted error bounds. We say that an analytic function $h: D_s \rightarrow \mathbb{C}^k$ is an analytic N -tail if the Taylor coefficients of h are zero to N -th order, i.e. if

$$h(z) = \sum_{|\alpha|=0}^{\infty} h_{\alpha} z^{\alpha},$$

and

$$h_{\alpha} = 0, \quad \text{for } 0 \leq |\alpha| \leq N.$$

Such functions are used to represent truncation errors in power series methods. For $p \in \mathbb{C}^k$ and $R > 0$ let

$$D_k(p, R) = \{z \in \mathbb{C}^k : \|z - p\| < R\},$$

We make the following assumptions.

A1: Assume that $f: D_k(p, R) \subset \mathbb{C}^k \rightarrow \mathbb{C}^k$ is analytic and that $p \in \mathbb{C}^k$ has $f(p) = p$.

A2: Assume that $Df(p)$ is nonsingular, diagonalizable, and hyperbolic. Let $\{\lambda_1, \dots, \lambda_s\}$ denote the stable eigenvalues, $\{\xi_1, \dots, \xi_s\}$ denote a choice of corresponding eigenvectors, Λ_s denote the $s \times s$ diagonal matrix of stable eigenvalues, and $A_s = [\xi_1, \dots, \xi_s]$ denote the $k \times s$ matrix whose columns are the stable eigenvectors.

A3: Assume that $P^N: \mathbb{C}^s \rightarrow \mathbb{C}^k$ is an N -th order polynomial, with $N \geq 2$. Assume that P^N is an exact formal solution of the equation

$$f \circ P^N = P^N \circ \Lambda_s,$$

to N -th order, that is, we assume that the power series of the right hand side is equal to the power series of the left hand side exactly up to N -th order.

The following definition collects some constants which are critical in the a-posteriori validation theorem to follow.

DEFINITION 3.7 (Validation values for the Stable Manifold). Let $f: \mathbb{C}^k \rightarrow \mathbb{C}^k$ and $P^N: \mathbb{C}^s \rightarrow \mathbb{C}^k$ be as in assumptions A1- A3. A collection of positive constants ϵ_{tol} , R , R' , μ^* , K_1 and K_2 are called *validation values* for P^N if

$$\sup_{z \in D_s} \|f[P^N(z)] - P^N(\Lambda_s z)\|_{\mathbb{C}^k} \leq \epsilon_{\text{tol}}, \quad (3.6)$$

$$\sup_{z \in D_s} \|P^N(z) - p\|_{\mathbb{C}^k} \leq R' < R, \quad (3.7)$$

$$0 < \max_{1 \leq j \leq s} |\lambda_j| \leq \mu^* < 1, \quad (3.8)$$

$$\sup_{z \in D_s} \|[Df]^{-1}(P^N(z))\| \leq K_1, \quad (3.9)$$

$$\max_{\substack{\beta \in \mathbb{N}^m \\ |\beta|=2}} \max_{1 \leq j \leq k} \sup_{q \in D_k(p, R)} \|\partial^\beta f_j(q)\|_{\mathbb{C}} \leq K_2. \quad (3.10)$$

Some explanation of the meaning of these constants is appropriate. In Equation (3.6), we see that ϵ_{tol} measures the defect associated with the approximation P^N on D_s . The requirement that $R' < R$ in Equation (3.7) guarantees that the image of the approximate parameterization P^N is contained in the disk $D_k(p, R')$, i.e. strictly interior to the disk $D_k(p, R)$ on which we have control over derivatives. The image of the true parameterization $P = P^N + H$ will live in the larger disk $D_k(p, R)$. Note that there is no assumption that either R' or R are small. Equation (3.8) postulates a uniform bound on the absolute values of the stable eigenvalues, while Equation (3.9)

requires a uniform bound on the inverse of the Jacobian derivative of f holding over all of D_s . Finally Equation (3.10) requires a uniform bound on the second derivatives of f which is valid over all of $D_k(p, R)$. Interval arithmetic computation of validation values is discussed in [25], and such computations are implemented for the Lomelí map in the same reference.

The following theorem is the main result of [25]. Its proof is found in the same reference.

THEOREM 3.8 (A-posteriori error bounds). *Given assumptions A1 – A3, suppose that ϵ_{tol} , R , R' , μ^* , K_1 , and K_2 are validation values for P^N . Let*

$$N_f = \#\{\beta \in \mathbb{N}^k : |\beta| = 2 \text{ and } \partial^\beta f_j(q) \neq 0 \text{ for } q \in D_k(p, R), 1 \leq j \leq k\},$$

count the number of not identically zero partial derivatives of f , and suppose that $N \in \mathbb{N}$ and $\delta > 0$ satisfy the three inequalities

$$N + 1 > \frac{-\ln(K_1)}{\ln(\mu^*)}, \quad (3.11)$$

$$\delta < e^{-1} \min \left(\frac{1 - K_1(\mu^*)^{N+1}}{2k\pi N_f K_1 K_2}, R - R' \right), \quad (3.12)$$

$$\frac{2K_1\epsilon_{\text{tol}}}{1 - K_1(\mu^*)^{N+1}} < \delta. \quad (3.13)$$

Then there is a unique analytic N -tail $h: D_m \subset \mathbb{C}^m \rightarrow \mathbb{C}^k$ having that

$$\sup_{z \in D_m} \|h(z)\|_{C^k} \leq \delta,$$

and that

$$P(z) = P^N(z) + h(z),$$

is the exact solution of Equation (3.2).

The theorem provides explicit conditions, all checkable by finite computations using interval arithmetic, sufficient to insure that there is an analytic N -tail so that $P^N + h$ solve the invariance equation for the Parameterization Method. In this case h is the truncation error on D_s associated with stopping our Taylor approximation at N -th order. δ then provides an explicit bound on the truncation error. Note also that the size of δ is related to the a-posteriori error ϵ_{tol} times the quantity K_1 , which in a sense measures how far from singular Df is on the image of P^N . The theorem also gives an indication of how large the order of approximation N must be taken.

In practice once validation values for P^N are found one then checks that N satisfies the condition given by Equation (3.11), computes a bound c_1 on the quantity given in the right hand side of Equation (3.12), computes a bound c_2 on the quantity given in the left hand side of Equation (3.13), and then checks that $c_1 > c_2$. Each of these computations and checks is done using interval arithmetic. If this procedure succeeds then the theorem holds for any $\delta \in (c_2, c_1)$. Of course in practice we then take δ as small as possible, i.e. very close to c_2 . Again these matters are discussed in more detail in [25].

REMARK 3.9 (Cauchy bounds on the derivative). Since the truncation error h is an analytic function bounded by δ on the fixed disk D_s , we can bound derivatives

of h on any smaller disk using classical estimates of complex analysis. Indeed, let $f: D_m(\nu) \rightarrow \mathbb{C}^k$ be an analytic function with

$$\sup_{z \in D_m(\nu)} \|f(z)\| \leq M.$$

Then for any $0 < \sigma \leq 1$ the Cauchy bounds

$$\sup_{z \in D_m(\nu e^{-\sigma})} \left\| \frac{\partial}{\partial z_j} f(z) \right\| \leq \frac{2\pi}{\nu\sigma} M,$$

translate bounds on the size of a function into bounds on the size of its derivative on a strictly smaller disk. An elementary proof of the Cauchy bounds can be found for example in [25]. Repeated application of the Cauchy bounds leads to estimates of j -th order derivatives inverse proportional to $(\nu\sigma)^j$.

Now suppose that P^N and $h, P: D_s \rightarrow \mathbb{C}^k$ are as in Theorem 3.8, so that $P(z) = P^N(z) + h(z)$ parameterizes a local stable manifold for p , and $\|h\| \leq \delta$ for $z \in D_s$. Then for $0 < \sigma \leq 1$, $z \in D_s$, and $1 \leq j \leq s$ we have that

$$\frac{\partial}{\partial z_j} P(z) = \frac{\partial}{\partial z_j} P^N(z) + \frac{\partial}{\partial z_j} h(z).$$

In practice the first term on the right is computed explicitly as the partial derivative of the known polynomial P^N , while the Cauchy bounds applied to the second term on the right yield that

$$\sup_{z \in D_s(e^{-\sigma})} \left\| \frac{\partial}{\partial z_j} h(z) \right\| \leq \frac{2\pi}{\sigma} \delta.$$

This decomposition is used in order to control derivatives of the truncation errors of the Parameterizations in the heteroclinic arc computations to follow. We just have to make sure that our heteroclinic arcs are contained in the interior of the domain D_s .

3.3. Example stable/unstable manifold computations. Figures 3.1 and 3.2 illustrate the results of several computations for the Lomelí map utilizing the Parameterization Method. Namely we compute polynomial approximations of the manifolds to order $N = 45$ for the two dimensional local unstable and stable manifolds at p_1 and p_2 respectively. The figures result from computing a triangular mesh in the domains of the parameterizations, and lifting the mesh to the phase space using the polynomial chart maps. Moreover, the global stable/unstable manifolds shown in Figure 1.1 are obtained from the local manifolds shown in Figure 3.1 after 30 iterates. Similarly, the global stable/unstable manifolds shown in Figure 1.2 are obtained from the local manifolds shown in Figure 3.2 after 10 iterates.

By verifying the hypotheses of Theorem 3.8 we obtain a-posteriori error bounds on the truncation error associated with the parameterizations. In all cases the supremum norm errors are confirmed to be smaller than 10^{-9} . These validated parameterizations are used in the sequel in order to study the heteroclinic arcs for the bubbles.

REMARK 3.10 (Software and performance). The parameterizations of all local stable and unstable manifolds used in the present work are computed and validated

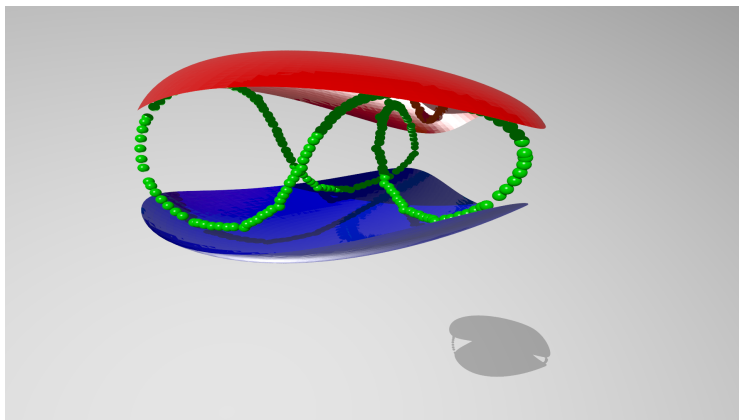


FIG. 3.1. *Local stable/unstable manifolds for the Lomelí map: images of polynomial parameterizations for the system with parameter values $a = 0.44$, $b = 0.21$, $c = 0.35$, $\alpha = -0.25$, and $\tau = -0.3$, i.e. the same parameters used to generate Figure 1.1. Local unstable manifold shown in blue and local stable manifold in red.*

using the INTLAB library for interval arithmetic running under MatLab [28]. Performance and implementation of the validated computations is discussed in detail in [25].

REMARK 3.11 (Dynamics inside the bubble). For the reader interested in the vortex bubble dynamics of the Lomelí map we have included some additional dynamical information in Figures 3.1 and 3.2. In addition to plotting the parameterized local stable/unstable manifolds we also considered a $500 \times 500 \times 500$ box of initial conditions in the “bubble region”. For the parameter values studied in Figure 3.1 we find that a typical orbit escapes the region (and diverges to infinity). The green trajectory in Figure 3.1 was found by considering only orbits which stay in the bubble region for more than 500 iterates. We conjecture that there is an unstable invariant circle near this green orbit.

For the parameter values studied in Figure 3.2 typical orbits in the “bubble region” are invariant tori, chaotic orbits, or orbits which escape the region all together. For example we plot as a green set in Figure 3.2 an orbit which appears to lie on an invariant torus.

4. Intersections of stable/unstable manifolds. In this section we discuss how to establish intersections of stable/unstable manifolds of hyperbolic fixed points.

Let $f : \mathbb{R}^k \rightarrow \mathbb{R}^k$ be an invertible map and p_1, p_2 its hyperbolic fixed points with associated stable manifolds $W^s(p_i)$ and unstable manifolds $W^u(p_i)$, for $i = 1, 2$. We assume that $W^u(p_1)$ is of dimension u_1 and that $W^s(p_2)$ is of dimension s_2 , with $m = u_1 + s_2 > k$. Our objective is to investigate the intersection of $W^u(p_1)$ with $W^s(p_2)$. We shall formulate conditions which ensure that they (locally) intersect transversally along an $m - k$ manifold in \mathbb{R}^k .

REMARK 4.1. *In the setting of the Lomelí map, we will have $k = 3$, $u_1 = s_2 = 2$*

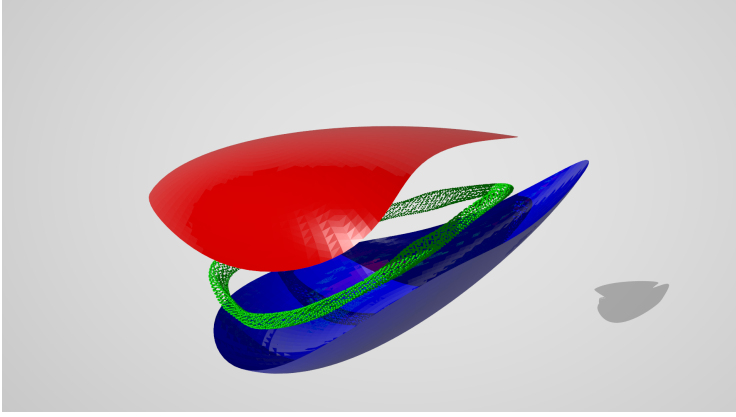


FIG. 3.2. *Local stable/unstable manifolds for the Lomelí map: images of polynomial parameterizations for the system with parameter values $a = 0.5$, $b = -0.5$, $c = 1$, $\alpha = -0.08999$, and $\tau = 0.8$, i.e. the same parameters used to generate Figure 1.2. Local unstable manifold shown in blue and local stable manifold in red.*

and so the manifolds will intersect along $u_1 + u_2 - k = 1$ dimensional curves. We write our method in the more general context, to emphasize that it is applicable also in higher dimensions.

We assume that the manifolds $W^u(p_1)$ and $W^s(p_2)$ are parameterized by

$$P_1 : B_{u_1} \rightarrow \mathbb{R}^k, \quad P_2 : B_{s_2} \rightarrow \mathbb{R}^k,$$

where B_{u_1} and B_{s_2} are used to denote balls centered at zero in \mathbb{R}^{u_1} and \mathbb{R}^{s_2} , respectively. We shall write θ for coordinates on \mathbb{R}^{u_1} and ϕ for coordinates on \mathbb{R}^{s_2} .

Let

$$\begin{aligned} F : B_{u_1} \times B_{s_2} &\rightarrow \mathbb{R}^k, \\ F(\theta, \phi) &= f^{l_1}(P_1(\theta)) - f^{-l_2}(P_2(\phi)), \end{aligned} \tag{4.1}$$

for some $l_1, l_2 \in \mathbb{N}$. We shall look for points $p^* \in B_u \times B_s$ for which we will have

$$F(p^*) = 0. \tag{4.2}$$

A point p^* satisfying (4.2) gives a point of intersection of $W^u(p_1)$ and $W^s(p_2)$ in the phase space as $P_1(\pi_\theta p^*)$, or $P_2(\pi_\phi p^*)$. The two points come from the same homoclinic orbit, i.e.

$$f^{l_1+l_2}(P_1(\pi_\theta p^*)) = P_2(\pi_\phi p^*).$$

We see that finding intersections of $W^u(p_1)$ and $W^s(p_2)$ reduces to finding zeros of F . In section 4.1 we address this problem in general context, and then apply the method to the Lomelí map in section 4.3.

4.1. General setup. Let us consider a function

$$F : \mathbb{R}^m \rightarrow \mathbb{R}^k,$$

where $m > k$. In this section we present an interval Newton type method for establishing estimates on the set

$$\Sigma_0 := \{F = 0\}. \quad (4.3)$$

If F is C^1 then we can expect Σ_0 to be a C^1 manifold of dimension $m - k$. Our method will work in such setting.

Consider $x \in \mathbb{R}^{m-k}$ and define a function $F_x : \mathbb{R}^k \rightarrow \mathbb{R}^k$ as

$$F_x(y) := F(x, y). \quad (4.4)$$

For $X \subset \mathbb{R}^{m-k}$ and $Y \subset \mathbb{R}^k$, by $DF_X(Y)$ we denote the family of matrixes

$$DF_X(Y) = \{D(F_x)(y) : x \in X, y \in Y\}.$$

Bounds on (4.3) can be obtained by using the interval Newton method. Below theorem is a well known modification (see for instance [29, p. 376]) of the method, that includes a parameter.

THEOREM 4.2. *Let $X = \Pi_{i=1}^{m-k} [a_i, b_i] \subset \mathbb{R}^{m-k}$ and $Y = \Pi_{i=1}^k [c_i, d_i] \subset \mathbb{R}^k$. Consider $y_0 \in \text{int}Y$ and*

$$N(y_0, X, Y) = y_0 - [DF_X(Y)]^{-1} [F_X(y_0)].$$

If

$$N(y_0, X, Y) \subset \text{int}Y, \quad (4.5)$$

then there exists a function $q : X \rightarrow Y$ such that $F(x, q(x)) = 0$.

REMARK 4.3. *By the implicit function theorem, $q(x)$ is as smooth as F .*

REMARK 4.4. *If we choose X to be a single point $X = \{x_0\}$, then we can use Theorem 4.2 to establish an enclosure $\{x_0\} \times Y$ of the point $(x_0, q(x_0))$, for which $F(x_0, q(x_0)) = 0$.*

REMARK 4.5. *In Theorem 4.2 we have fixed x to be the first k coordinates. We can also apply the method by fixing any other k of the m coordinates.*

For X, Y from Theorem 4.2, the set $X \times Y$ is an enclosure of Σ_0 . The theorem establishes the smoothness of Σ_0 and proves that it is a graph over the X coordinate. This approach to obtaining an enclosure is simple and direct, but has one major flaw. The main issue is that the bound on $F_X(y_0) = F(X, y_0)$ might not be tight, and in such case the application of the method would require a choice of very small X . This in practice could result in needing a vast number of sets to fully enclose Σ_0 . A natural remedy for keeping the enclosure of $F_X(y_0)$ in check would be a more careful choice of local coordinates. This is what motivates our next approach.

Assume that p^* is a point for which we have

$$F(p^*) = 0. \quad (4.6)$$

We will consider a neighborhood of p^* , in which we want to locally enclose Σ_0 . Let A_1 be a $m \times (m - k)$ matrix and let A_2 be a $m \times k$ matrix. We will be looking for points of the form

$$p = p(x, y) := p^* + A_1 x + A_2 y$$

for which

$$F(p(x, y)) = 0. \quad (4.7)$$

We will first formulate an interval Newton-type theorem that will allow us to establish bounds on x, y solving (4.7). Later we will follow with comments on how A_1 and A_2 should be chosen and why the proposed approach can provide better estimates than Theorem 4.2.

THEOREM 4.6. *Let A_1 be an $m \times (m - k)$ matrix and let A_2 be a $m \times k$ matrix. Let $X = \Pi_{i=1}^{m-k} [a_i, b_i]$, $Y = \Pi_{i=1}^k [c_i, d_i]$, $x_0 \in X$, $y_0 \in Y$ and let us introduce the following notations*

$$\begin{aligned} F_{x_0, y_0} &:= F(p^* + A_1 x_0 + A_2 y_0), \\ DF_{X, y_0} &:= DF(p^* + A_1 X + A_2 y_0), \\ DF_{X, Y} &:= DF(p^* + A_1 X + A_2 Y), \\ N(x_0, y_0, A_1, A_2, X, Y) &:= y_0 - [DF_{X, Y} A_2]^{-1} (F_{x_0, y_0} + [DF_{X, y_0} A_1] [X - x_0]). \end{aligned} \quad (4.8)$$

If

$$N(x_0, y_0, A_1, A_2, X, Y) \subset Y,$$

then there exists a function $q : X \rightarrow Y$, such that

$$F(p^* + A_1 x + A_2 q(x)) = 0. \quad (4.9)$$

Moreover, q is as smooth as F .

Proof. Let us introduce the following notation. Let $g_x : Y \rightarrow \mathbb{R}^k$ and $h : X \rightarrow \mathbb{R}^k$ be defined as

$$\begin{aligned} g_x(y) &= F(p^* + A_1 x + A_2 y), \\ h(x) &= F(p^* + A_1 x + A_2 y_0). \end{aligned}$$

By the mean value theorem, for any $x \in X$

$$\begin{aligned} g_x(y_0) &= h(x) \\ &\in h(x_0) + [Dh(X)] [X - x_0] \\ &= F_{x_0, y_0} + [DF_{X, y_0} A_1] [X - x_0]. \end{aligned}$$

Also for any $x \in X$,

$$[Dg_x(Y)] = [DF(p^* + A_1 x + A_2 Y) A_2] \subset [DF_{X, Y} A_2].$$

This means that for any $x \in X$

$$y_0 - [Dg_x(Y)]^{-1} [g_x(y_0)] \subset N(x_0, y_0, A_1, A_2, X, Y) \subset Y,$$

hence by the interval Newton theorem for every $x \in X$ we have $q(x)$ for which $g_x(q(x)) = 0$. This means that

$$F(p^* + A_1 x + A_2 q(x)) = g_x(q(x)) = 0.$$

To prove that $q(x)$ is smooth, consider $g : X \times Y \rightarrow \mathbb{R}^m$ defined as

$$g(x, y) = F(p^* + A_1x + A_2y).$$

Since $g(x, y) = g_x(y)$ we see that $g(x, q(x)) = 0$. This means that in order to prove that $q(x)$ is smooth it is enough to show that for any $x \in X$ and $y \in Y$ the matrix $\frac{\partial g}{\partial y}(x, y)$ is invertible (smoothness then follows from the implicit function theorem). Since $\frac{\partial g}{\partial y} = Dg_x \in [DF_{X,Y}A_2]$, we see that the matrix must be invertible, since for $N(x_0, y_0, A_1, A_2, X, Y)$ to be well defined we have implicitly assumed that any matrix in $[DF_{X,Y}A_2]$ is invertible. \square

Now we comment on the choice of A_1, A_2 and discuss why Theorem 4.6 is better than Theorem 4.2.

REMARK 4.7. When Σ_0 is a C^1 manifold of dimension $m-k$, then since $F(\Sigma_0) = 0$, we see that for a point $p \in \Sigma_0$ the tangent space $T_p\Sigma_0$ to Σ_0 at p is an $m-k$ dimensional space, which lies in the kernel of $DF(p)$. We can take A_1 whose columns consist of vectors which span $T_p\Sigma_0$. The image of A_1 is then $T_p\Sigma_0$, and for any $v \in \mathbb{R}^{m-k}$, $DF(p)A_1v = 0$. Then, provided that X is a small set, $[DF_{X,y_0}A_1][X - x_0]$ should be small. This means that by incorporating A_1 in the setup of local coordinates improves the deficiency of Theorem 4.2.

REMARK 4.8. Once A_1 is chosen we can choose A_2 as any matrix of rank k so that the image of A_2 is orthogonal to A_1 .

REMARK 4.9. In practice, the candidate for a set Y can be found automatically by iterating the operator N several times.

REMARK 4.10. In our computer assisted proof, when applied to the Lomelí map, we have found that Theorem 4.6 works better than the direct approach from Theorem 4.2. To give an indication of the difference between the two: If we were to take the interval enclosure of $p^* + A_1x + A_2q(x)$, i.e.

$$\tilde{X} \times \tilde{Y} := [p^* + A_1X + A_2Y],$$

consider a mid point y_0 of \tilde{Y} , and compute $N(y_0, \tilde{X}, \tilde{Y})$, then in our computer assisted validation the diameter of the set $N(y_0, \tilde{X}, \tilde{Y})$ turns out to be up to thirty times larger than the diameter of \tilde{Y} . Thus, we would not be able to validate (4.5). The validation using Theorem 4.6 does go through.

COROLLARY 4.11. By differentiating (4.9) we see that

$$DF(p^* + A_1x + A_2q(x))(A_1 + A_2Dq(x)) = 0,$$

hence

$$Dq(x) \in -[DF_{X,Y}A_2]^{-1}[DF_{X,Y}A_1].$$

This means that we can obtain bounds with computer assistance on the derivative of $q(x)$.

We shall now use Theorem 4.6 to establish intersections of stable/unstable manifolds. Recall that F was defined using (4.1). Let us introduce the following notation. For $q(x)$ from Theorem 4.6 let $\theta : X \rightarrow \mathbb{R}^{u_1}$ and $\phi : X \rightarrow \mathbb{R}^{s_2}$ be defined as

$$\begin{aligned} \theta(x) &= \pi_\theta(p^* + A_1x + A_2q(x)), \\ \phi(x) &= \pi_\phi(p^* + A_1x + A_2q(x)). \end{aligned}$$

(This means that $(\theta(x), \phi(x)) = p^* + A_1x + A_2q(x)$.) Also, let $p : X \rightarrow \mathbb{R}^k$ be defined as

$$p(x) = f^{l_1}(P_1(\theta(x))).$$

THEOREM 4.12. *Assume that F is defined by (4.1), and that assumptions of Theorem 4.6 are fulfilled. Then the manifolds $W^u(p_1)$ and $W^s(p_2)$ intersect transversally along $p(x)$ for $x \in X$. Moreover, $p(x)$ is as smooth as f .*

Proof. By Theorem 4.6,

$$0 = F(p^* + A_1x + A_2q(x)) = f^{l_1}(P_1(\theta(x))) - f^{-l_2}(P_2(\phi(x))),$$

meaning that

$$p(x) := f^{l_1}(P_1(\theta(x))) = f^{-l_2}(P_2(\phi(x))).$$

Since $P_1(\theta(x)) \in W^u(p_1)$ and $P_2(\phi(x)) \in W^s(p_2)$, we see that $W^u(p_1)$ and $W^s(p_2)$ intersect at $p(x)$.

We now address the issue of transversality. Consider a $k \times u_1$ matrix C_1 and a $k \times s_2$ matrix C_2 defined as

$$\begin{aligned} C_1 &= \frac{d}{d\theta} f^{l_1}(P_1(\theta(x))), \\ C_2 &= \frac{d}{d\phi} f^{-l_2}(P_2(\phi(x))), \end{aligned}$$

and observe that

$$\begin{aligned} T_{p(x)} W^u(p_1) &= \{C_1 v : v \in \mathbb{R}^{u_1}\}, \\ T_{p(x)} W^s(p_2) &= \{C_2 w : w \in \mathbb{R}^{s_2}\}. \end{aligned}$$

To prove that $W^u(p_1)$ and $W^s(p_2)$ intersect transversally, we need to show that

$$\{C_1 v + C_2 w : v \in \mathbb{R}^{u_1}, w \in \mathbb{R}^{s_2}\} = \mathbb{R}^k. \quad (4.10)$$

Since assumptions of Theorem 4.6 hold, the matrix $DF(\theta(x), \phi(x)) A_2$ is invertible. Observing that

$$DF(\theta(x), \phi(x)) A_2 = C_1 \pi_\theta A_2 - C_2 \pi_\phi A_2,$$

invertibility implies that for any $p \in \mathbb{R}^k$ there exists a $y \in \mathbb{R}^k$ such that

$$C_1 \pi_\theta A_2 y - C_2 \pi_\phi A_2 y = p.$$

Above equation implies (4.10).

The $p(x)$ is smooth, since it is a composition of smooth functions. This concludes the proof. \square

4.2. Establishing intersections of manifolds along curves. We now show how to use the method to establish a bound for a curve along which F is zero. This example will later be used by us to establish one dimensional curves along intersections of $W^u(p_1)$ and $W^s(p_2)$ in the Lomelí map.

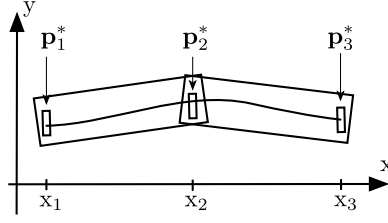


FIG. 4.1. The enclosure of a curve from section 4.2.

We will use bold font to denote interval enclosures of sets. This means that all notations in bold represent interval sets (cubes), and operations performed on them are in interval arithmetic.

Let B_1, B_2, \dots, B_{N+1} be a sequence of cubes in \mathbb{R}^{m-1} , and let $x_1, x_2, \dots, x_{N+1} \in \mathbb{R}$. We consider a sequence of sets $\mathbf{p}_1^*, \dots, \mathbf{p}_{N+1}^*$, of the form

$$\mathbf{p}_n^* = \{x_n\} \times B_n \quad \text{for } n = 1, \dots, N+1. \quad (4.11)$$

(See Figure 4.1.) Using Theorem 4.2 (taking $X = \{x_n\}$ and $Y = B_n$), we can establish that \mathbf{p}_n^* contain zeros of F . Our objective will be to obtain a bound on the curve along which F is zero, which joins the points in $\mathbf{p}_1^*, \dots, \mathbf{p}_{N+1}^*$.

Let $\mathbf{A}_{1,n} = \mathbf{p}_{n+1}^* - \mathbf{p}_n^*$. Consider $X = [0, 1]$, consider a sequence of closed $m-1$ dimensional cubes Y_1, \dots, Y_N in \mathbb{R}^{m-1} and a sequence of matrixes $A_{2,1}, \dots, A_{2,N}$. We can choose these so that the range of $A_{2,n}$ is (roughly) orthogonal to the range of $\mathbf{A}_{1,n}$, for $n = 1, \dots, N$. Such choice can easily be automated. The choice of Y_n can also be automated, by iterating the Newton operator defined in (4.8).

REMARK 4.13. Note that $\mathbf{p}_{n+1}^*, \mathbf{p}_n^*$ are on the curve which we wish to establish. This means that $\mathbf{A}_{1,n} = \mathbf{p}_{n+1}^* - \mathbf{p}_n^*$ is close to the tangent space of the curve. This by Remark 4.7 means that such $\mathbf{A}_{1,n}$ should be a good choice, meaning that we should have

$$[DF(\mathbf{p}_n^*)]\mathbf{A}_{1,n}x \approx 0, \quad \text{for } x \in [0, 1].$$

Let $x_0 \in X$, $y_{0,n} \in Y_n$ be the mid points of the sets X and Y_n , respectively. Assume that for any $A_{1,n} \in \mathbf{A}_{1,n}$ and $p_n^* \in \mathbf{p}_n^*$, assumptions of Theorem 4.6 hold for $X, Y_n, x_0, y_{0,n}, A_{1,n}, A_{2,n}, p_n^*$. If this is true for $n = 1, \dots, N$, then from Theorem 4.6 it follows that there exists a curve joining the points in $\mathbf{p}_1^*, \dots, \mathbf{p}_{N+1}^*$ on which F is zero. The curve is contained in the set

$$\bigcup_{n=1}^N \{\mathbf{p}_n^* + \mathbf{A}_{1,n}x + A_{2,n}y : x \in [0, 1], y \in Y_n\}.$$

Above procedure can be summed up as follows:

Algorithm.

Input: A sequence of points p_1, \dots, p_{N+1} , for which $F(p_n) \approx 0$, for $n = 1, \dots, N+1$. (These points can be computed non-rigorously.)

Output: A sequence of sets:

$$\{\mathbf{p}_n^* + \mathbf{A}_{1,n}x + A_{2,n}y : x \in [0, 1], y \in Y_n\},$$

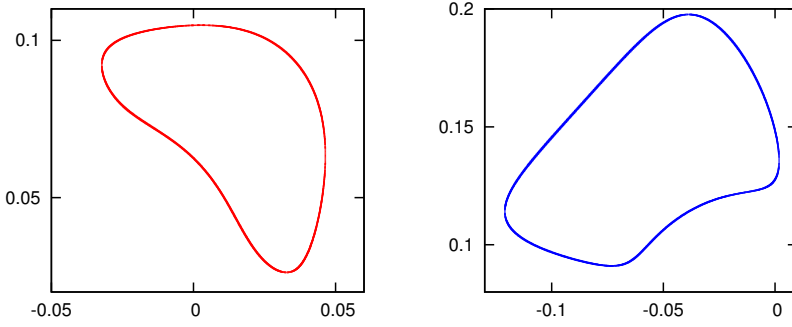


FIG. 4.2. The enclosure of a heteroclinic loop in the parameter space. On the left we have the projection onto B_s (in red) and on the right the projection onto B_u (in blue). Here we considered the Lomelí map with $a = \frac{1}{2}$, $b = -\frac{1}{2}$, $c = 1$, $\alpha = -0.08999$, $\tau = \frac{8}{10}$.

which enclose the curve on which F is zero.

Steps:

1. Enclose p_1, \dots, p_{N+1} in sets $\mathbf{p}_1^*, \dots, \mathbf{p}_{N+1}^*$ of the form (4.11) and validate existence of zeros of F inside of $\mathbf{p}_1^*, \dots, \mathbf{p}_{N+1}^*$ using Theorem 4.2 and Remark 4.4.
2. For $\mathbf{A}_{1,n} = \mathbf{p}_{n+1}^* - \mathbf{p}_n^*$, choose $m \times m - 1$ matrixes, for which the range of $A_{2,i}$ is (roughly) orthogonal to $\mathbf{A}_{1,n}$.
3. Take $X = [0, 1]$, $x_0 = \frac{1}{2}$, $y_0 = 0$ and $Y_1 = \dots = Y_N = \{0\}$. Iterate the Newton operator (4.8) several times and enlarge each Y_n .
4. For $n = 1, \dots, N$, validate assumptions of Theorem 4.6 for

$$X, Y_n, x_0, y_0^n, \mathbf{A}_{1,n}, A_{2,n}, \mathbf{p}_n^*.$$

4.3. Application to the Lomelí map. In this section we apply the method from section 4.2 to the Lomelí map. Here we establish a computer assisted proof of two types of intersections. The first type is when the stable and unstable manifolds intersect along closed curves, which is the setting from Figure 1.2. Such intersections are established in section 4.3.1. The second type of intersection is along heteroclinic arcs, as is the case in Figure 1.1. Such arcs are established in section 4.3.2.

4.3.1. Heteroclinic loops. In this section we consider the Lomelí map (2.1) with parameters $a = \frac{1}{2}$, $b = -\frac{1}{2}$, $c = 1$, $\alpha = -0.08999$, $\tau = \frac{8}{10}$ and give a computer assisted proof of a connection of $W^u(p_1)$ with $W^s(p_2)$ along a heteroclinic loop. Such loop generates, by iterates of f , the intersections of $W^u(p_1)$ and $W^s(p_2)$, which are shown in Figure 1.2.

We consider

$$F : B_u \times B_s \rightarrow \mathbb{R}^3$$

defined as

$$F(\theta, \phi) = f^{l_1}(P_1(\theta)) - f^{-l_2}(P_2(\phi)), \quad (4.12)$$

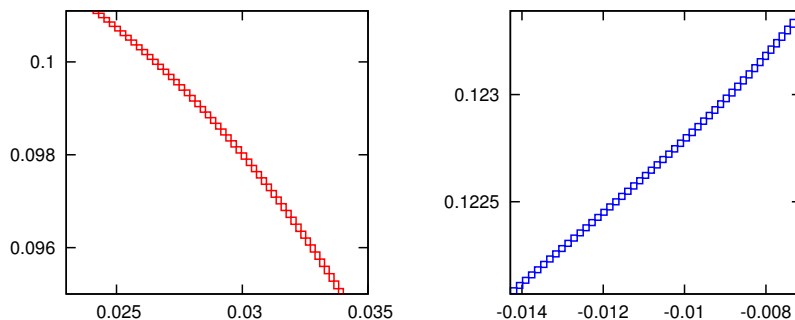


FIG. 4.3. The closeup of the enclosure of a heteroclinic loop from Figure 4.2.

with $l_1 = l_2 = 9$.

REMARK 4.14. We point out that (4.12) involves many compositions of the map f . Computing such compositions directly in interval arithmetic leads to a blowup. This is associated with the fact that enclosing each iterate in a rectangular box produced overestimates; the so called wrapping effect. (For more information on the wrapping effect see [30].) If we were to naively compose f in interval arithmetic, then the below obtained results would not go through. For our computation of interval enclosure of F and DF we use a careful, Lohner-type set representation, that reduces the wrapping effect when computing bounds on f^k and Df^k . This representation is discussed in detail in section 4.4.

We follow the procedure from section 4.2 to establish the enclosure of the curve in the parameter space $B_u \times B_s$. Our curve is enclosed using $N = 1309$ small cubes in \mathbb{R}^4 . Figure 4.2 consists of these cubes, but this is not visible from the plot. After magnification the cubes start to take shape. In Figure 4.3 we show a close-up of 50 of such cubes. (The total number of considered cubes results from a non-rigorous procedure, which we have used to find initial points that are close to the intersection of the manifolds. They are the input of the Algorithm from page 23. The $N = 1309$ is arbitrary, and we could have chosen a different number.)

We can propagate the loop in the parameter space using the linear inner dynamics. This way we obtain the plot from Figure 4.4. This figure corresponds to the intersections visible in Figure 1.2. The difference is that the loops in Figure 4.2 are in the parameter space and the loops from Figure 1.2 are in the state space. Our bounds on the inner dynamics are rigorous. They follow from the parameterisation method (see (3.2) and Remark 3.2). Thus, the resulting plots from Figure 4.4 are also rigorous enclosures of the curves, as long as we remain within the domains of our parameterisations. The boundary of the domain is depicted in green. Thus, the part of the plot which is within the green boundary is rigorous.

The computation needed to establish the heteroclinic loop took 59 seconds on a single 3GHz Intel i7 core processor, running on MacBook Pro, with OS X 10.9.5. We have conducted our proof using c++ and the CAPD¹ library. For the computational environment used to obtain the local stable/unstable parameterizations we refer to Remark 3.10.

¹Computer Assisted Proofs in Dynamics: <http://capd.ii.uj.edu.pl/>

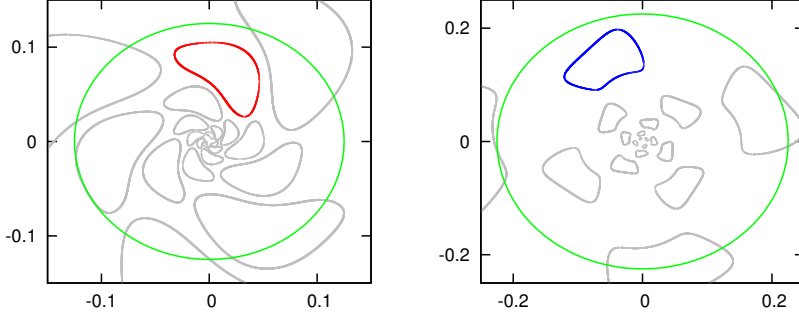


FIG. 4.4. The loop from Figure 4.2 propagated using the linear inner dynamics on the parameter space. In green we have the boundaries of the domains of the parameterisations.

4.3.2. Heteroclinic arcs. In this section we consider the Lomelí map with parameters $a = \frac{44}{100}$, $b = \frac{21}{100}$, $c = \frac{35}{100}$, $\alpha = -\frac{1}{4}$, $\tau = -\frac{3}{10}$ and give a computer assisted proof of a connection of $W^u(p_1)$ with $W^s(p_2)$ along two 3-fold primary heteroclinic arcs, which lead to six homoclinic paths from p_1 to p_2 .

We consider F as defined in (4.12). Applying Theorem 4.2 together with Remark 4.4, we establish $N = 309$ enclosures of points $\mathbf{p}_1^*, \dots, \mathbf{p}_N^*$ on which F is zero. (The number of considered points is arbitrary; as long as the validation would go through we could take a different N .) The dynamics on the unstable and stable manifolds is conjugated with a linear map

$$\begin{aligned} f \circ P_1(\theta) &= P_1(A_1\theta), \\ f \circ P_2(\phi) &= P_2(A_2\phi), \end{aligned}$$

where

$$A_i = \begin{pmatrix} \operatorname{re}\lambda_i & -\operatorname{im}\lambda_i \\ \operatorname{im}\lambda_i & \operatorname{re}\lambda_i \end{pmatrix} \quad \text{for } i = 1, 2,$$

and λ_1, λ_2 are the eigenvalues of $Df(p_1)$ and $Df(p_2)$, respectively. We have established the following bounds for the eigenvalues

$$\begin{aligned} \operatorname{re}\lambda_1 &\in \mathbf{re}\lambda_1 = [-0.71570025199987, -0.71570025199985], \\ \operatorname{im}\lambda_1 &\in \mathbf{im}\lambda_1 = [-0.93025058966104, -0.93025058966103], \end{aligned}$$

$$\begin{aligned} \operatorname{re}\lambda_2 &\in \mathbf{re}\lambda_2 = [-0.47875667823481, -0.47875667823480], \\ \operatorname{im}\lambda_2 &\in \mathbf{im}\lambda_2 = [-0.70015090953401, -0.70015090953400]. \end{aligned}$$

We consider interval matrixes

$$\begin{aligned} \mathbf{A}_i &= \begin{pmatrix} \mathbf{re}\lambda_i & -\mathbf{im}\lambda_i \\ \mathbf{im}\lambda_i & \mathbf{re}\lambda_i \end{pmatrix}, \quad \text{for } i = 1, 2, \\ \mathbf{B} &= \begin{pmatrix} \mathbf{A}_1 & 0 \\ 0 & \mathbf{A}_2 \end{pmatrix}, \end{aligned}$$

and take

$$\mathbf{p}_{N+1}^* = \mathbf{B}^3 \mathbf{p}_1^*.$$

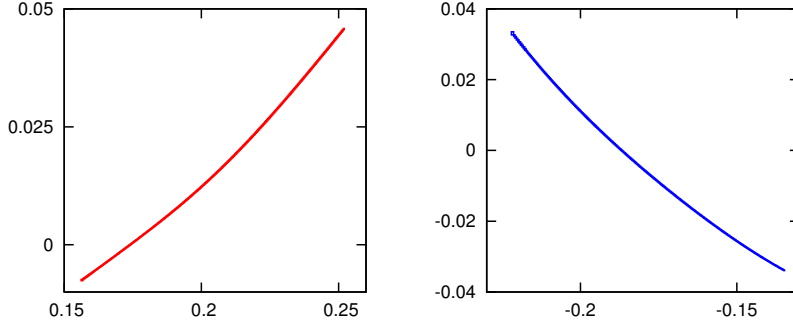


FIG. 4.5. *Enclosure of a fundamental heteroclinic arc. On the left we have the projection onto B_s (in red) and on the right the projection onto B_u (in blue). Here we considered the Lomelí map with $a = \frac{44}{100}$, $b = \frac{21}{100}$, $c = \frac{35}{100}$, $\alpha = -\frac{1}{4}$ and $\tau = -\frac{3}{10}$.*

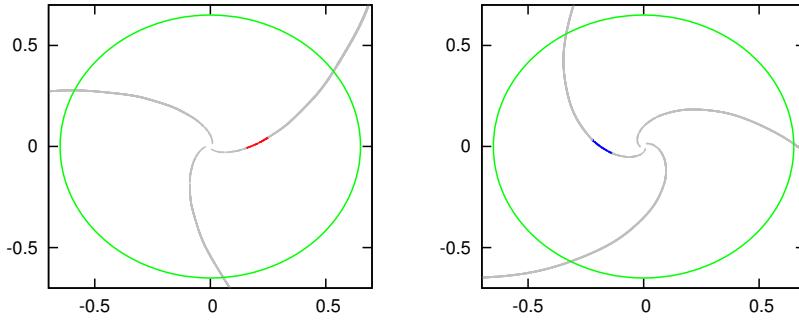


FIG. 4.6. *Enclosures of heteroclinic paths in parameter space. In blue and red we have the fundamental heteroclinic arc from Figure 4.5. All three gray homoclinic paths are obtained by iterates of the single fundamental heteroclinic arc. In green we have the boundaries of the domains of the parameterisations.*

Following the method from section 4.2, we establish an enclosure of a curve (in parameter space) $\gamma = (\gamma_u, \gamma_s) \subset B_u \times B_s$, which passes through $\mathbf{p}_1^*, \mathbf{p}_2^*, \dots, \mathbf{p}_{N+1}^*$. The enclosure is shown in Figure 4.5.

The path γ can be iterated by the linear dynamics in the parameter space. A couple of such iterates result in a picture from Figure 4.6.

Since we took $\mathbf{p}_{N+1}^* = \mathbf{B}^3 \mathbf{p}_1^*$, the $P_1(\gamma_u)$ and $P_2(\gamma_s)$ are 3-fold fundamental heteroclinic arcs (as discussed in case 2 from Section 2.3) and we obtain a heteroclinic path:

$$S_3 = S_3(P_1(\gamma_u)) = \bigcup_{i \in \mathbb{Z}} f^{3i}(P_1(\gamma_u)).$$

REMARK 4.15. *Since we know that $F(\gamma) = 0$, by (4.12),*

$$f^9(P_1(\gamma_u)) - f^{-9}(P_2(\gamma_s)) = 0,$$

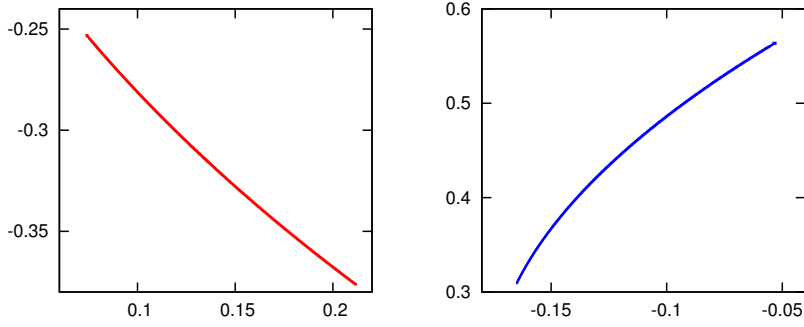


FIG. 4.7. *Enclosure of the second fundamental heteroclinic arc for the Lomelí map with $a = \frac{44}{100}$, $b = \frac{21}{100}$, $c = \frac{35}{100}$, $\alpha = -\frac{1}{4}$ and $\tau = -\frac{3}{10}$. On the left we have the projection onto B_s (in red) and on the right the projection onto B_u (in blue).*

and thus

$$S_3 = \bigcup_{i \in \mathbb{Z}} f^{3i}(P_1(\gamma_u)) = \bigcup_{i \in \mathbb{Z}} f^{3i}(P_2(\gamma_s)).$$

Also $f(S_3)$ and $f^2(S_3)$ are heteroclinic paths. Thus the 3-fold fundamental heteroclinic arc γ generates three paths. These three paths lie on the intersection of the stable and unstable manifolds from Figure 1.1.

For the investigated parameters, one can find a second 3-fold fundamental heteroclinic arc that generates a different set of three homoclinic paths. We have obtained its enclosure using the same procedure, by considering $N = 344$ cubes. The obtained enclosure is given in Figure 4.7. We can propagate this arc using the linear inner dynamics on the parameter space (see (3.2) and Remark 3.2), and obtain the plot in Figure 4.8. Since we have rigorous bounds on the inner dynamics, the resulting plots are rigorous, as long as the estimates stay within the domains of the parameterisations.

As a result, we obtain six homoclinic paths in total, which form the intersections of the stable and unstable manifolds shown in Figure 1.1. The paths from Figure 4.8 are in the parameter space, and the paths in Figure 1.1 are in the state space.

The computation needed to establish the two fundamental heteroclinic arcs took 27 seconds on a single 3GHz Intel i7 core processor, running on MacBook Pro, with OS X 10.9.5. Our proof has been implemented in c++, using the CAPD² library. For the computational environment used to obtain the local stable/unstable parameterizations we refer to Remark 3.10.

4.4. Controlling the wrapping effect. In the computer assisted proofs from Sections 4.3.1, 4.3.2 we have established the connections of the manifolds by investigating $F = 0$, where F was given by (4.12). This F involves many compositions of the Lomelí map f . To apply Theorem 4.6 we need good estimates on interval enclosure of F and DF computed on sets. If this is computed directly in interval arithmetic by composing f and Df many times, then the wrapping effect significantly reduces the accuracy of the computations. In order to overcome the wrapping effect, one can

²Computer Assisted Proofs in Dynamics: <http://capd.ii.uj.edu.pl/>

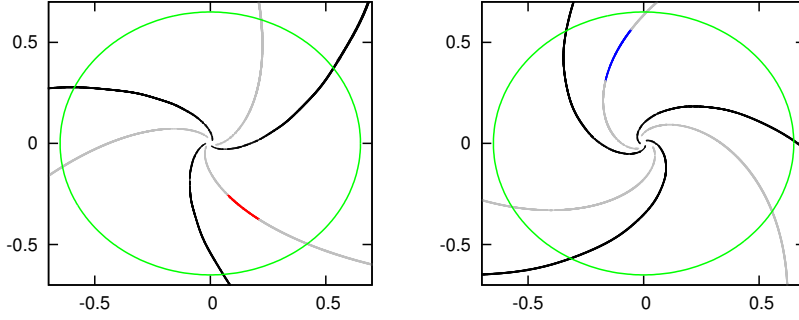


FIG. 4.8. In gray, the enclosures of three homoclinic paths generated by the second fundamental heteroclinic arc. In black, the previous three paths from Figure 4.6. The second fundamental heteroclinic arc from Figure 4.7 is in red and blue. In green we have the boundaries of the domains of the parameterisations.

use multiple shooting or good set representation. In our approach we have chosen the second approach.

We use a Lohner type representation for images and derivatives by the map f . The approach is in the spirit of [31], but simpler since we consider a map instead of integrating an ODE.

To discuss our set representation we need some auxiliary notations. In this section we shall use the calligraphic font \mathcal{A} to denote sequences of matrixes

$$\mathcal{A} = (A_1, \dots, A_n).$$

In our setting, A_i will be $n \times n$ Hessians matrixes. (For the Lomelí map $n = 3$.) For $b \in \mathbb{R}^n$ we will write $b^T \mathcal{A}$ to denote an $n \times n$ matrix and $b^T \mathcal{A} b$ to denote a vector, defined as follows:

$$b^T \mathcal{A} = \begin{pmatrix} b^T A_1 \\ \vdots \\ b^T A_n \end{pmatrix}, \quad b^T \mathcal{A} b = \begin{pmatrix} b^T A_1 b \\ \vdots \\ b^T A_n b \end{pmatrix}. \quad (4.13)$$

(Each $b^T A_i$ is a $1 \times n$ matrix, which constitutes the i -th row of the $n \times n$ matrix $b^T \mathcal{A}$.) We will also use a convention in which for a matrix B we shall write $B\mathcal{A}$ and $\mathcal{A}B$ for sequences of matrixes defined as follows:

$$B\mathcal{A} = (BA_1, \dots, BA_n) \quad \text{and} \quad \mathcal{A}B = (A_1B, \dots, A_nB).$$

For an $n \times n$ matrix $B = (B_{ki})_{k,i=1}^n$ we define a sequence of matrixes $B * \mathcal{A}$ as follows

$$B * \mathcal{A} = \left(\sum_{i=1}^n B_{1i} A_i, \dots, \sum_{i=1}^n B_{ni} A_i \right).$$

We now give a technical lemma, which will be useful later on.

LEMMA 4.16. For any \mathcal{A} , B and b ,

$$B(b^T \mathcal{A}) = b^T (B * \mathcal{A}). \quad (4.14)$$

Proof. The result follows from direct computation. We write out the proof in the appendix. \square

For $h : \mathbb{R}^n \rightarrow \mathbb{R}$, let ∇h stand for the gradient of h and let $\nabla^2 h$ stand for the Hessian of h .

The Lomelí map f is quadratic, which means that

$$\begin{aligned} f_i(x_0 + b) &= f_i(x_0) + Df_i(x_0)b + \frac{1}{2}b^T (\nabla^2 f_i) b, \\ \nabla f_i(x_0 + b) &= \nabla f_i(x_0) + (\nabla^2 f_i) b. \end{aligned}$$

If we choose $\mathcal{H} = (\nabla^2 f_1, \dots, \nabla^2 f_n)$, then using our notations (4.13), we can rewrite the above as (for the second equality below we use the fact that $Df_i(x) = (\nabla f_i(x))^T$)

$$\begin{aligned} f(x_0 + b) &= f(x_0) + Df(x_0)b + \frac{1}{2}b^T \mathcal{H}b, \\ Df(x_0 + b) &= Df(x_0) + b^T \mathcal{H}. \end{aligned} \tag{4.15}$$

In our computer assisted consideration, we will represent points as

$$x_0 + Ab + r,$$

and derivatives as

$$X_0 + b^T \mathcal{A} + R,$$

meaning that in interval representation

$$x \in x_0 + A\mathbf{b} + \mathbf{r}, \tag{4.16}$$

$$X \in X_0 + \mathbf{b}^T \mathcal{A} + \mathbf{R}, \tag{4.17}$$

where \mathbf{b} and \mathbf{r} are interval vectors and \mathbf{R} is an interval matrix. Below we show why such representation is a good idea. (Its main objective is to reduce the wrapping effect.)

We take a point of the form

$$x = x_0 + u \quad \text{with } u = Ab + r, \tag{4.18}$$

and compute

$$\begin{aligned} f_i(x) &= f_i(x_0) + Df_i(x_0)u + \frac{1}{2}u^T (\nabla^2 f_i) u \\ &= f_i(x_0) + Df_i(x_0)Ab + Df_i(x_0)r + \frac{1}{2}(Ab + r)^T (\nabla^2 f_i) (Ab + r). \end{aligned}$$

From the above we see that if $b \in \mathbf{b}$ and $r \in \mathbf{r}$, then

$$f(x) \in f(x_0) + (Df(x_0)A)\mathbf{b} + Df(x_0)\mathbf{r} + \frac{1}{2}(A\mathbf{b} + \mathbf{r})^T \mathcal{H}(A\mathbf{b} + \mathbf{r}),$$

meaning that

$$f(x) \in \tilde{x}_0 + \tilde{A}\mathbf{b} + \tilde{\mathbf{r}}, \tag{4.19}$$

for

$$\begin{aligned}\tilde{x}_0 &= f(x_0), \\ \tilde{A} &= Df(x_0)A, \\ \tilde{\mathbf{r}} &= Df(x_0)\mathbf{r} + \frac{1}{2}(A\mathbf{b} + \mathbf{r})^T \mathcal{H}(A\mathbf{b} + \mathbf{r}).\end{aligned}$$

REMARK 4.17. We note that the second term in $\tilde{\mathbf{r}}$ is $O(\|A\mathbf{b} + \mathbf{r}\|^2)$. This means that if \mathbf{r} is $O(\|\mathbf{b}\|^2)$, then $\tilde{\mathbf{r}}$ will also be $O(\|\mathbf{b}\|^2)$. The \tilde{x}_0 can be computed with good accuracy, since we do not need to evaluate f on a large set, but just at a single point. Similarly, $Df(x_0)$ can be computed accurately, and so in turn will be \tilde{A} .

REMARK 4.18. If we split up our computation of $\tilde{\mathbf{r}}$ into

$$\tilde{\mathbf{r}} = Df(x_0)\mathbf{r} + \frac{1}{2}(\mathbf{b}^T(A^T\mathcal{H}A)\mathbf{b} + \mathbf{b}^T(A^T\mathcal{H})\mathbf{r} + \mathbf{r}^T(\mathcal{H}A)\mathbf{b} + \mathbf{r}^T\mathcal{H}\mathbf{r}),$$

then the wrapping effect will be reduced even more.

We now show how our representation works when computing derivatives. We consider x of the form (4.18) and a matrix X of the form

$$X = X_0 + b^T\mathcal{A} + R.$$

Below we will compute $Df(x)X$. Using (4.15) for the first equality below, and Lemma 4.16 for the third, we see that

$$\begin{aligned}Df(x)X &= \left(Df(x_0) + \left((Ab + r)^T \mathcal{H}\right)\right)X \\ &= Df(x_0)[X_0 + b^T\mathcal{A} + R] + \left((Ab + r)^T \mathcal{H}\right)[X_0 + b^T\mathcal{A} + R] \\ &= Df(x_0)X_0 + b^T(Df(x_0) * \mathcal{A} + A^T\mathcal{H}X_0) \\ &\quad + r^T\mathcal{H}X_0 + Df(x_0)R + \left((Ab + r)^T \mathcal{H}\right)(b^T\mathcal{A} + R).\end{aligned}$$

This means that for $b \in \mathbf{b}$, $R \in \mathbf{R}$ and $r \in \mathbf{r}$

$$Df(x)X \in \tilde{X}_0 + \mathbf{b}^T\tilde{\mathcal{A}} + \tilde{\mathbf{R}}, \quad (4.20)$$

for

$$\begin{aligned}\tilde{X}_0 &= Df(x_0)X_0, \\ \tilde{\mathcal{A}} &= Df(x_0) * \mathcal{A} + A^T\mathcal{H}X_0, \\ \tilde{\mathbf{R}} &= \mathbf{r}^T\mathcal{H}X_0 + Df(x_0)\mathbf{R} + (A\mathbf{b} + \mathbf{r})^T \mathcal{H}(\mathbf{b}^T\mathcal{A} + \mathbf{R}).\end{aligned}$$

REMARK 4.19. As in Remark 4.17, we see that \tilde{X}_0 and $\tilde{\mathcal{A}}$ can be computed accurately. Moreover, if \mathbf{r} and \mathbf{R} are $O(\|\mathbf{b}\|^2)$ then $\tilde{\mathbf{R}}$ will also be $O(\|\mathbf{b}\|^2)$.

The representation (4.16–4.17) is intended to control the wrapping effect for computing $f^k(x)$ and $Df^k(x)$ for larger $|k|$. To compute a bound for $f^k(\mathbf{x})$ and $Df^k(\mathbf{x})$ in our representation, we start with a set enclosure and with identity matrix:

$$\begin{aligned}\mathbf{x} &= x_0 + \mathbf{b}, \\ X &= Id,\end{aligned} \quad (4.21)$$

meaning that we start with $A = Id$, $\mathbf{r} = 0$, $X_0 = Id$, $\mathbf{R} = 0$ and $\mathcal{A} = 0$ in the representations of a set (4.16) and derivative (4.17). We then iterate the map using (4.19) and (4.20). The resulting set enclosure will be of the form

$$f^k(\mathbf{x}) \subset x_k + A_k \mathbf{b} + \mathbf{r}_k, \quad (4.22)$$

for some vector x_k , some matrix A_k , and some interval vector \mathbf{r}_k , that follow from our iterative procedure.

REMARK 4.20. *The \mathbf{b} in (4.22) is the same as in (4.21), which is the main objective of our representation. By Remark 4.17, the x_k and A_k can be computed accurately, and we can expect \mathbf{r}_k to be small.*

The enclosure of the derivative at the end of our iterative procedure will be

$$Df^k(\mathbf{x}) \subset X_k + \mathbf{b}^T \mathcal{A}_k + \mathbf{R}_k, \quad (4.23)$$

for some matrix X_k , some sequence of matrixes \mathcal{A}_k , and some interval matrix \mathbf{R}_k , that follow from our iterative procedure.

REMARK 4.21. *The \mathbf{b} in (4.22) is the same as the one in (4.21). By Remark 4.19, we can expect \mathbf{R}_k to be small, and the X_k , \mathcal{A}_k can be computed accurately.*

Above method of representing sets works quite nicely in our case, since the Lomeli map is quadratic. The method though can also be applied in more general setting:

REMARK 4.22. *To apply our method the map f does not need to be quadratic. It is enough to have interval enclosures \mathbf{H}_i of the second derivatives on a set U ,*

$$\mathbf{H}_i = \left[\left\{ A \in \mathbb{R}^n \times \mathbb{R}^n \mid A_{jk} \in \left[\inf_{x \in U} \frac{\partial^2 f_i}{\partial x_j \partial x_k}(x), \sup_{x \in U} \frac{\partial^2 f_i}{\partial x_j \partial x_k}(x) \right] \right\} \right],$$

for the set U containing $x = x_0 + Ab + r$. We can then use the \mathbf{H}_i instead of $\nabla^2 f_i$ in our computations. This gives a method for the computation of bounds on iterates of maps and on their derivatives, which reduces the wrapping effect.

5. Acknowledgements. We are grateful for useful discussions to J. L. Figueras, W. Tucker and D. Wilczak. We would like to thank the two anonymous reviewers for their suggestions and comments, which helped us to improve the manuscript.

6. Appendix. *Proof.* (of Lemma 4.16) We use the fact that

$$b^T A_m = \left(\sum_j b_j A_{mj1} \quad \sum_j b_j A_{mj2} \quad \dots \quad \sum_j b_j A_{mjn} \right),$$

hence the coefficient with index ik in the matrix $b^T \mathcal{A}$ has the form

$$(b^T \mathcal{A})_{mk} = \sum_j b_j A_{mj k}. \quad (6.1)$$

This allows us to compute the left hand side of (4.14) as (we use (6.1) in the second equality, in the first we simply multiply matrixes)

$$(B(b^T \mathcal{A}))_{ik} = \sum_m B_{im} (b^T \mathcal{A})_{mk} = \sum_{m,j} B_{im} b_j A_{mj k}.$$

To compute the right hand side of (4.14), we first observe that the i -th matrix in $B * \mathcal{A}$ is

$$(B * \mathcal{A})_i = \sum_m B_{im} A_m. \quad (6.2)$$

We now compute the right hand side of (4.14) as, (we use (6.1) in the first equality, and (6.2) in the second equality)

$$\begin{aligned} (b^T (B * \mathcal{A}))_{ik} &= \sum_j b_j (B * \mathcal{A})_{ijk} = \sum_j b_j \left(\sum_m B_{im} A_m \right)_{jk} \\ &= \sum_j b_j \sum_m (B_{im} A_m)_{jk} = \sum_{j,m} b_j B_{im} A_{mjk}. \end{aligned}$$

Both sides of (4.14) are the same, which finishes our proof. \square

REFERENCES

- [1] S. Smale. Differentiable dynamical systems. *Bull. Amer. Math. Soc.*, 73:747–817, 1967.
- [2] J. D. Meiss. Thirty years of turnstiles and transport. *Chaos*, 25(9):097602, September 2015.
- [3] X. Cabré, E. Fontich, and R. de la Llave. The parameterization method for invariant manifolds. I. Manifolds associated to non-resonant subspaces. *Indiana Univ. Math. J.*, 52(2):283–328, 2003.
- [4] X. Cabré, E. Fontich, and R. de la Llave. The parameterization method for invariant manifolds. II. Regularity with respect to parameters. *Indiana Univ. Math. J.*, 52(2):329–360, 2003.
- [5] X. Cabré, E. Fontich, and R. de la Llave. The parameterization method for invariant manifolds. III. Overview and applications. *J. Differential Equations*, 218(2):444–515, 2005.
- [6] À. Haro and R. de la Llave. A parameterization method for the computation of invariant tori and their whiskers in quasi-periodic maps: numerical algorithms. *Discrete Contin. Dyn. Syst. Ser. B*, 6(6):1261–1300 (electronic), 2006.
- [7] A. Haro and R. de la Llave. A parameterization method for the computation of invariant tori and their whiskers in quasi-periodic maps: rigorous results. *J. Differential Equations*, 228(2):530–579, 2006.
- [8] Gianni Arioli and Hans Koch. Computer-assisted methods for the study of stationary solutions in dissipative systems, applied to the Kuramoto-Sivashinski equation. *Arch. Ration. Mech. Anal.*, 197(3):1033–1051, 2010.
- [9] Sarah Day, William D. Kalies, and Thomas Wanner. Verified homology computations for nodal domains. *Multiscale Model. Simul.*, 7(4):1695–1726, 2009.
- [10] Sarah Day, Jean-Philippe Lessard, and Konstantin Mischaikow. Validated continuation for equilibria of PDEs. *SIAM J. Numer. Anal.*, 45(4):1398–1424 (electronic), 2007.
- [11] Marcio Gameiro, Jean-Philippe Lessard, and Alessandro Pugliese. Computation of smooth manifolds of solutions of PDEs via rigorous multi-parameter continuation. *Found. Comput. Math.*, 16(2):531–575, April 2016.
- [12] Konstantin Mischaikow and Thomas Wanner. Probabilistic validation of homology computations for nodal domains. *Ann. Appl. Probab.*, 17(3):980–1018, 2007.
- [13] Jan Bouwe van den Berg, Jean-Philippe Lessard, and Konstantin Mischaikow. Global smooth solution curves using rigorous branch following. *Math. Comp.*, 79(271):1565–1584, 2010.
- [14] J. D. Mireles James and Hector Lomelí. Computation of heteroclinic arcs with application to the volume preserving Hénon family. *SIAM J. Appl. Dyn. Syst.*, 9(3):919–953, 2010.
- [15] J. D. Mireles James. Quadratic volume-preserving maps: (un)stable manifolds, hyperbolic dynamics, and vortex-bubble bifurcations. *J. Nonlinear Sci.*, 23(4):585–615, 2013.
- [16] Maciej Capiński and J. D. Mireles James. Web page for the paper *validated computation of heteroclinic arcs*. <http://cosweb1.fau.edu/~jmirelesjames/validatedArcsPage.html>.
- [17] Anatole Katok and Boris Hasselblatt. *Introduction to the modern theory of dynamical systems*, volume 54 of *Encyclopedia of Mathematics and its Applications*. Cambridge University Press, Cambridge, 1995. With a supplementary chapter by Katok and Leonardo Mendoza.
- [18] Clark Robinson. *Dynamical systems*. Studies in Advanced Mathematics. CRC Press, Boca Raton, FL, 1995. Stability, symbolic dynamics, and chaos.
- [19] P. J. Archer, T. G. Thomas, and G. N. Coleman. Direct numerical simulation of vortex ring evolution from the laminar to the early turbulent regime. *J. Fluid Mech.*, 598:201–226, 2008.
- [20] R. S. MacKay. Transport in 3D volume-preserving flows. *J. Nonlinear Sci.*, 4(4):329–354, 1994.
- [21] Fotis Sotiropoulos, Yiannis Ventikos, and Tahiri C. Lackey. Chaotic advection in three-dimensional stationary vortex-breakdown bubbles: Silnikov’s chaos and the devil’s staircase. *J. Fluid Mech.*, 444:257–297, 2001.

- [22] H. R. Dullin and J. D. Meiss. Quadratic volume-preserving maps: invariant circles and bifurcations. *SIAM J. Appl. Dyn. Syst.*, 8(1):76–128, 2009.
- [23] K. E. Lenz, H. E. Lomelí, and J. D. Meiss. Quadratic volume preserving maps: an extension of a result of Moser. *Regul. Chaotic Dyn.*, 3(3):122–131, 1998. J. Moser at 70 (Russian).
- [24] Héctor E. Lomelí and James D. Meiss. Quadratic volume-preserving maps. *Nonlinearity*, 11(3):557–574, 1998.
- [25] J. D. Mireles James and Konstantin Mischaikow. Rigorous a posteriori computation of (un)stable manifolds and connecting orbits for analytic maps. *SIAM J. Appl. Dyn. Syst.*, 12(2):957–1006, 2013.
- [26] Maxime Breden, Jean-Philippe Lessard, and Jason D. Mireles James. Computation of maximal local (un)stable manifold patches by the parameterization method. *Indag. Math. (N.S.)*, 27(1):340–367, 2016.
- [27] J. B. Van den Berg, J. D. Mireles James, and Christian Reinhardt. A parameterized newton-kantorovich method for rigorously computing (un)stable manifolds: non-resonant and resonant spectra. (*In preperation*).
- [28] S.M. Rump. *INTLAB - INTerval LABoratory*. Kluwer Academic Publishers, Dordrecht, 1999.
- [29] Siegfried M. Rump. Verification methods: rigorous results using floating-point arithmetic. *Acta Numer.*, 19:287–449, 2010.
- [30] Ramon E. Moore. *Methods and applications of interval analysis*, volume 2 of *SIAM Studies in Applied Mathematics*. Society for Industrial and Applied Mathematics (SIAM), Philadelphia, Pa., 1979.
- [31] Piotr Zgliczynski. C^1 Lohner algorithm. *Found. Comput. Math.*, 2(4):429–465, 2002.